

Cover Page



Universiteit Leiden



The handle <http://hdl.handle.net/1887/77740> holds various files of this Leiden University dissertation.

Author: Kuo, C.L.

Title: Applications for activity-based probes in biomedical research on glycosidases

Issue Date: 2019-09-10

CHAPTER 5

Development and application of activity-based probes for α -L-iduronidase

Manuscript published as:

Artola M, **Kuo CL**, McMahon SA, Oehler V, Hansen T, van der Lienden M, He X, van den Elst H, Florea BI, Kermode AR, van der Marel GA, Gloster TM, Codée JDC, Overkleeft HS & Aerts JMF^G (2018) New Irreversible α -l-Iduronidase Inhibitors and Activity-Based Probes. *Chemistry* **24**, 19081–19088.

ABSTRACT

Human α -L-iduronidase is a retaining exo-acting glycosidase responsible for catalyzing the lysosomal turnover of glycosaminoglycans, and its hereditary deficiency underlies the lysosomal storage disorder mucopolysaccharidosis type I (MPS I). New covalent inhibitors and ABPs of α -L-iduronidase has been synthesized based on the cyclophellitol scaffold, and these were shown to react covalently and irreversibly in an activity-based manner with human recombinant α -L-iduronidase (rIDUA, Aldurazyme[®]), albeit with a lower potency and slower inhibitory kinetics compared to earlier generated ABPs towards other retaining glycosidases. The structures of IDUA when complexed with the inhibitors in a noncovalent transition-state-mimicking form and a covalent enzyme-bound form provide insights into its conformational itinerary. Inhibitors **1–3** adopt a half-chair conformation in solution ($^4\text{H}_3$ and $^3\text{H}_4$), as predicted by DFT calculations, which is different from the conformation of the Michaelis complex observed by crystallographic studies. Consequently, **1–3** may need to overcome an energy barrier in order to switch from the $^4\text{H}_3$ conformation to the transition state ($^2, ^5\text{B}$) binding conformation before reacting and adopting a covalent $^5\text{S}_1$ conformation, explaining their lower potency and slower inhibitory kinetics. Nevertheless, rIDUA can be efficiently labeled with fluorescent Cy5 ABP **2**, which allows monitoring of the delivery of this therapeutic recombinant enzyme to lysosomes, as is intended in enzyme replacement therapy for the treatment of MPS I patients.

5.1 Introduction

Human α -L-iduronidase (IDUA), which belongs to the GH39 family in the Carbohydrate Active EnZyme (CAZy) classification,^{1, 2} hydrolyzes terminal non-reducing α -L-iduronic acid residues in glycosaminoglycans (GAGs), including dermatan sulfate (DS) and heparan sulfate (HS), through a two-step Koshland double-displacement mechanism (**Fig. 5.1A**).^{3–6} The active site of the enzyme contains a carboxylic acid/carboxylate pair that acts as an acid/base (Glu188) and a nucleophilic (Glu299) catalyst. Protonation of the exocyclic oxygen by the acid/base residue and concomitant nucleophilic attack at the anomeric carbon by Glu299 leads to S_N2 displacement of the aglycon, yielding a covalent enzyme–substrate complex with inversion of stereochemistry at the anomeric carbon. In the next step, a water molecule enters the enzyme active site, where it is deprotonated by the acid/base (Glu188) and then hydrolyzes the enzyme–substrate intermediate in a reversal of steps, again with inversion of anomeric configuration. The conformational change of IDUA from Michaelis complex to transition state (TS) and enzyme–inhibitor covalent complex has recently been suggested to follow a $^2S_0 \rightarrow ^2, ^5B \rightarrow ^5S_1$ itinerary.^{5, 7, 8} This catalytic pathway was predicted on the basis of the structures of Michaelis complexes with (2R, 3R, 4R, 5S)-2-carboxy-3,4,5-trihydroxypiperidine (IdoA-DNJ) and 5-fluoro- α -L-idopyranosyluronic acid fluoride (5F-IdoAF) as reversible inhibitors and the 2-deoxy-2-fluoro- α -L-idopyranosyluronic acid (2F-IdoA)–enzyme covalent complex intermediate.

Mutations in the gene encoding IDUA may result in mucopolysaccharidosis type I (MPS I), which is a rare autosomal inherited recessive disease that leads to toxic accumulation of HS and DS. MPS I is a devastating disease that affects around 1 in 100,000 individuals and is classified as attenuated MPS I and more severe MPS I (traditionally categorized from less to more severe form as Scheie, Hurler–Scheie, or Hurler disease) to distinguish between disease severity and therapeutic options.⁸ Children with severe MPS I are treated at a young age by hematopoietic cell transplantation (HCT).⁹ Enzyme replacement therapy (ERT) with recombinant human α -L-iduronidase (rIDUA, Aldurazyme®) is considered as a treatment for non-neurological manifestations of MPS I.¹⁰ There is consensus among treating clinicians that

the impact of ERT with rIDUA is greatest when the treatment is initiated early in the disease progression. An obvious prerequisite for effectiveness is the successful targeting of infused rIDUA to lysosomes in multiple cell types, and for this purpose a detailed understanding of rIDUA targeting is still urgently needed. Besides MPS I, lysosomal α -L-iduronidase is indirectly involved in two other inherited lysosomal storage disorders, mucopolipidosis II (ML II) and III a/b. Here, a deficiency in the generation of mannose-6-phosphate (M6P) moieties in N-linked glycans of newly formed lysosomal enzymes impairs their correct routing to lysosomes and therefore these, including α -L-iduronidase, are largely erroneously secreted.¹¹

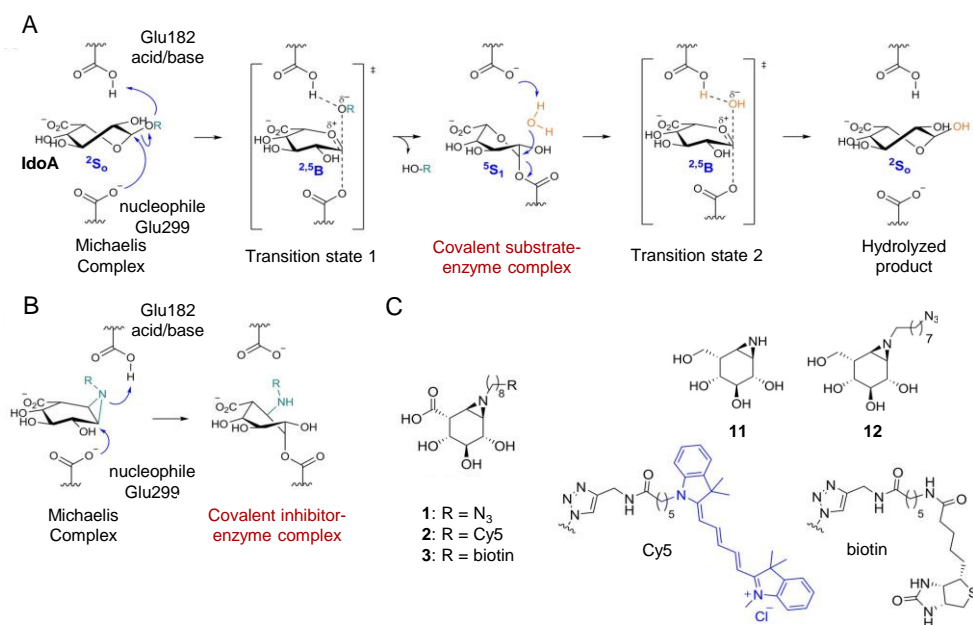


Figure 5.1. Reaction mechanisms and structures of compounds used in this chapter. A) Koshland double-displacement mechanism employed by retaining α -L-iduronidase, showing the $^2S_0 \rightarrow ^{2.5}B \rightarrow ^5S_1$ conformational reaction itinerary from the Michaelis complex, transition state 1, covalent substrate-enzyme intermediate, and transition state 2, to the hydrolyzed product. B) Proposed inhibition mechanism of aziridine-based inhibitor **1** and ABPs **2** and **3**. C) Chemical structures of α -L-iduronic-configured mechanism-based irreversible inhibitor **1** and ABPs **2** and **3**, and the idose-configured compound **11** and **12** described in this work.

Herein, the characterization and application of new irreversible IDUA inhibitors and activity-based probes (ABPs) bearing an α -L-iduronic configured cyclophellitol aziridine as an electrophilic “warhead” is reported. Functionalization of the aziridine with a Cy5 fluorophore

(for gel and/or cell imaging) or biotin (for chemical proteomics studies) afforded valuable tools (**Fig. 5.1B, C**) for the study of α -L-iduronidase *in vitro* and *in situ*, structural analysis, and for monitoring rIDUA uptake and trafficking to lysosomes, as is revealed in this chapter.

5.2 Results

5.2.1 Synthesis of α -L-iduronic-configured inhibitors and ABPs

The synthetic strategy for compound **1**, ABP **2** and ABP **3** (**Fig. 5.1C**) (Department of Bio-organic Synthesis, Leiden University) is described in detail in section 4.S1.2 in the **Appendix**. Briefly, to obtain the desired α -L-iduronic-configured inhibitors and ABPs, the α -L-iduronic-configured cyclohexene **8** was produced in three steps, followed by benzylation of free alcohol and aziridination with 3-amino-2-(trifluoromethyl)quinazolin-4(3*H*)-one (CF₃-Q-NHOAc), following strategy described by Llebaria and coworkers¹² and the Overkleeft group¹³ (**Scheme 5.S1**). After removal of benzyl and CF₃-Q groups, the obtained idose-configured aziridine **11** (**Fig. 5.1C**) was alkylated to afford the azide-containing compound **12** (**Fig. 5.1C**), which was further oxidized at C-6 to afford the α -L-iduronic-configured cyclophellititol aziridine compound **1** (**Fig. 5.1C**). Finally, click reaction with a Cy5- or biotin-substituted alkyne on compound **1** afforded the desired ABP **2** or **3** (**Fig. 5.1C**).

5.2.2 *In vitro* inhibition and labeling of recombinant human α -L-iduronidase with compounds **1–3**

The *in vitro* inhibition potencies of compounds **1–3** was examined by incubating them for 60 min at various inhibitor concentrations with human recombinant α -L-iduronidase (rIDUA, Genzyme) at pH 4.5, followed by 30 min incubation with the fluorogenic substrate 4-methylumbelliferyl- α -iduronide (4-MU-IdoA). The assay mixture was supplemented with BSA, Triton X-100, NaCl, and chloride salt of divalent cations, by adapting methods described in literatures^{14, 15}, which resulted in a 3.5-fold increase in rIDUA activity (**Fig. 5.S1**). Compounds **1–3** inhibited rIDUA with apparent half-maximum inhibitory concentrations in the micromolar range (**Fig. 5.2**). Intermediate **11** showed no activity (**Fig. 5.2**), in line with the role of the

carboxylate group at C5 for IDUA binding in a positively charged enzymatic pocket formed by the Arg363 and Lys264 side chains and the main-chain NH groups of Gly305 and Trp306.⁸ Surprisingly, alkyl aziridine **12** inhibited rIDUA on a par with compound **1–3** (Fig. 5.2), suggesting that the carboxylate group may not be essential for binding if an N-alkyl group is presented. These results are also in line with previous findings that N-alkyl aziridines display improved binding potency towards glycosidases.¹⁶

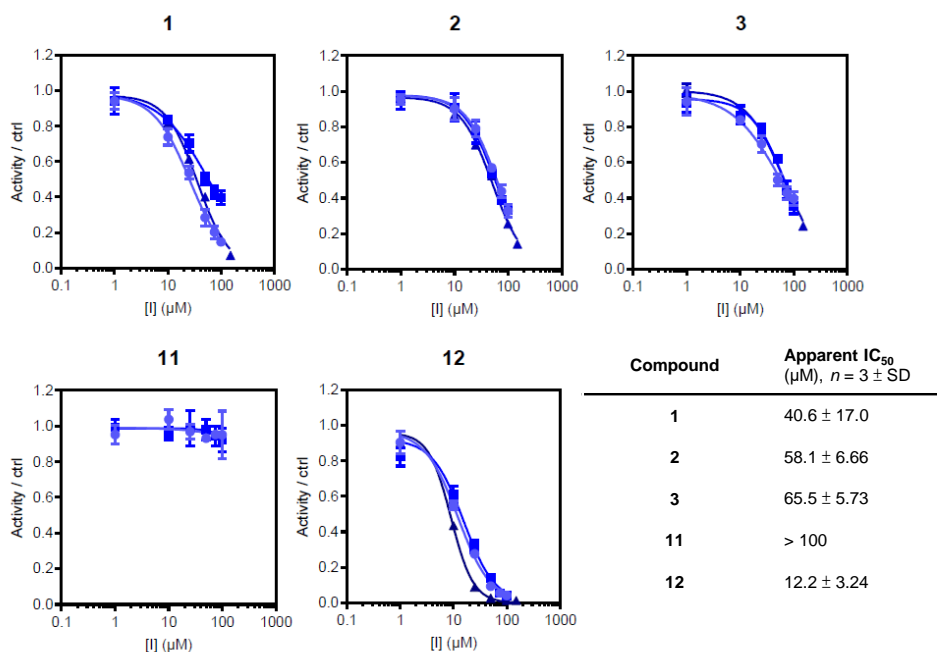


Figure 5.2. *In vitro* inhibition of recombinant α -L-iduronidase (rIDUA) by compounds **1–3**, **11** and **12** at 1 hour incubation time. Compounds **1–3**, **12** = triplicate sets of experiment, each with technical triplicates; **11** = duplicate sets of experiment. Error range in inhibition curves = SD from technical triplicates. Error range in IC_{50} values = SD from triplicate (or duplicate) experimental sets.

Cy5 ABP **2** labeled rIDUA in a concentration- and time-dependent manner, consistent with the irreversible inhibition mechanism of these analogues, with optimal labeling at 50μ M and about 120–180 min incubation, as visualized by SDS-PAGE (Fig. 5.3A). The optimum pH for labeling with ABP **2** was determined as 4.5–5.0, consistent with the reported optimum pH for enzymatic activity (Fig. 5.3B).² The stability of the covalent enzyme–inhibitor complex was

also tested, and it was observed that rIDUA remained inactivated for at least 100 h (Fig. 5.3C). In addition, competitive activity-based protein profiling (ABPP) showed competition in a

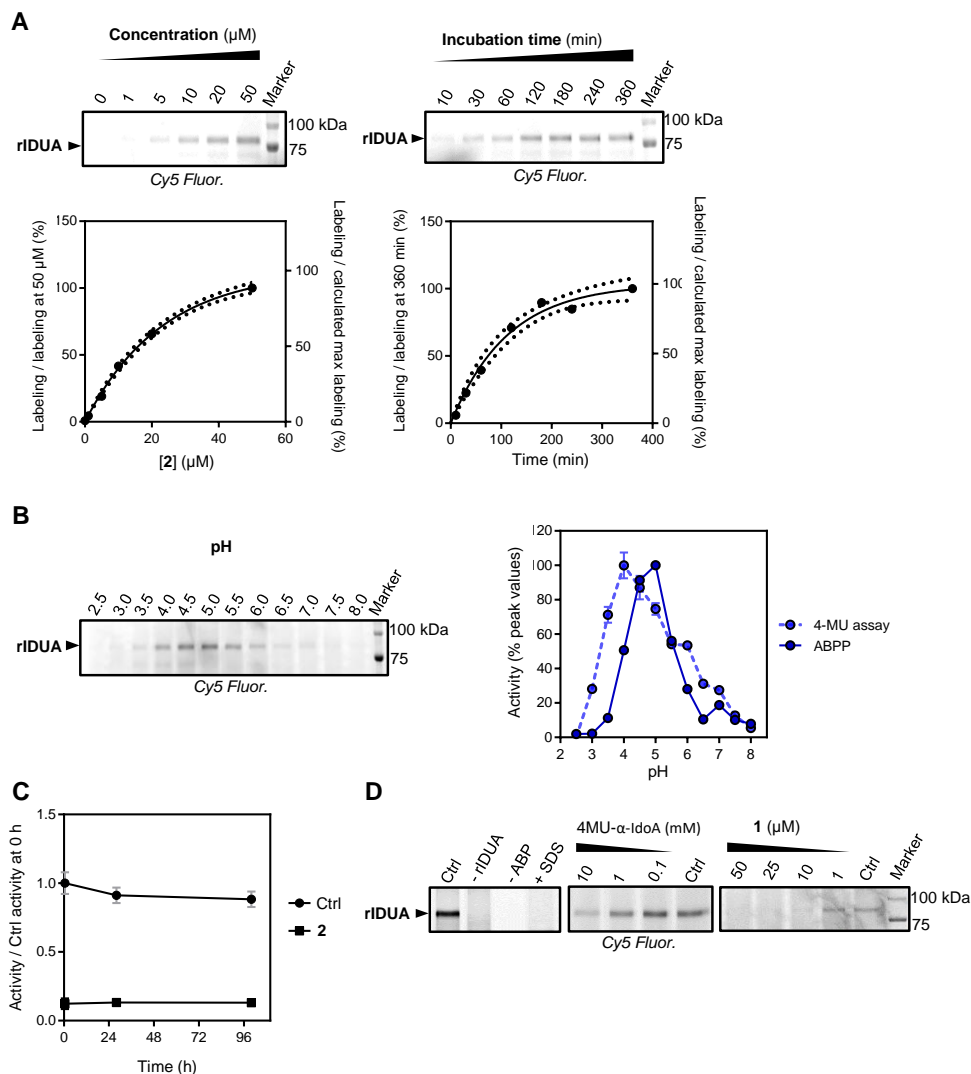


Figure 5.3. Labeling of rIDUA with ABPs 2. A) Cy5 ABP 2 labels rIDUA (10 ng) in a concentration-dependent (left, at 4 h incubation time) and time-dependent (right, at 50 μM) manner. Labeling signals were quantified (below each gel image) and fitted with a one-phase association equation. Dotted lines represent 95 % CI. B) ABP 2 labels rIDUA in a pH-dependent manner. The quantified labeling signals were compared to data obtained with 4-MU substrate assay (below; error range =SD from technical triplicates). C) Irreversible inhibition of rIDUA by ABP 2. Error range = SD from technical triplicates. D) ABP 2 labels rIDUA and negative controls: without rIDUA, without ABP 2 or with SDS (left panel), competition with 4-MU-α-L-iduronic acid (middle panel) or 1 (right panel).

concentration-dependent manner with 4-MU-IdoA as well as with inhibitor **1**, illustrating the applicability of this probe for the screening of new inhibitors (**Fig. 5.3D**).

Next, kinetic parameters for rIDUA labeling/inhibition by ABP **2** was determined. Due to the fluorescent nature and the slow labeling on rIDUA by ABP **2** (**Fig. 4.3A**, right panel), it was envisioned that kinetic parameters could be derived by monitoring the progress of rIDUA labeling by ABP **2** at various concentrations (5–60 μ M) and different incubation times (30–150 min) using an SDS-PAGE-based ABPP method. This would simplify the derivatization of kinetic parameters commonly applied for irreversible inhibitors (see Experimental procedures **5.4.9** for more detailed explanation). Indeed, when labeling of rIDUA by ABP **2** (**Fig. 5.S2**) was quantified (**Fig. 5.4A**), the initial binding constant (K_I) and an inactivation rate constant (k_{inact}) could be determined (**Fig. 5.4B**). The calculated k_{inact}/K_I value was $1.38 \times 10^{-4} \mu\text{M}^{-1} \text{min}^{-1}$,

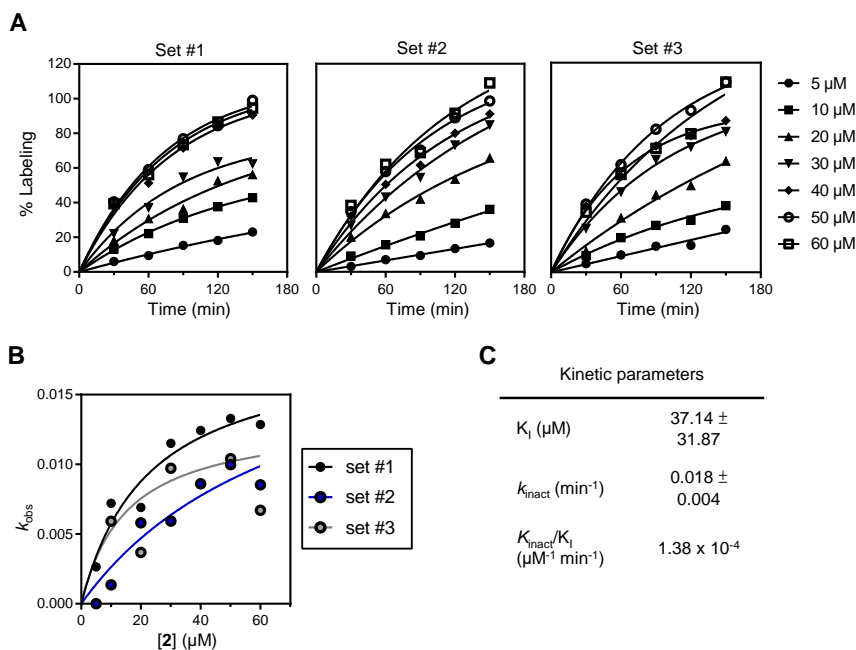


Figure 5.4. Kinetic parameters for ABP 2 towards rIDUA. A) Percentages of rIDUA labeling at different time points and at different concentrations of ABP **2**. Data were quantified from three sets of fluorescent gels containing rIDUA labeled with ABP **2** under the depicted conditions to derive a rate constant k for each ABP **2** concentration. B) Left, k vs. [inhibitor] plot. Data were curve-fitted with the Michaelis–Menten equation to obtain kinetic parameters. Right, calculated kinetic parameters for ABP **2** labeling of rIDUA. Error range = SD from the three sets.

showing this compound to be a less potent inactivator than other ABPs for related glycosidases, such as β -glucuronidases¹⁶, β -glucosidases^{17, 18}, α -glucosidases¹⁹, and α -galactosidase²⁰.

To further demonstrate the covalent binding to the catalytically active amino acid, biotinylated ABP **3** was incubated with rIDUA, and peptide mass fingerprinting-based proteomic was utilized to detect for the presence of ABP **3** on the active site peptide of rIDUA. After ABP incubation, rIDUA was denatured and digested by chymotrypsin, and the resulting ABP **3**-labeled peptides were affinity-enriched and analyzed by nanoscale liquid chromatography coupled with tandem mass spectrometry (nano-LC-MS/MS). A fragment of the IDUA nucleophile (Glu299) covalently attached to ABP **3** was detected by MS/MS fragmentation of the 7-amino-acid peptide containing the nucleophilic residue (**Fig. 5.5**, **5.S3** and **5.S4**).

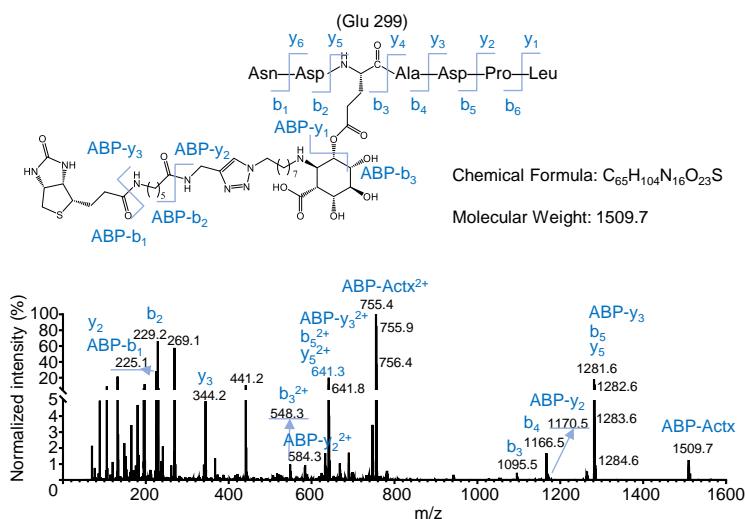


Figure 5.5. Proteomic detection of ABP 3-labeled rIDUA peptides. MS/MS pattern of a sample containing rIDUA Asn297–Leu303 active site peptide labeled with biotin ABP **3** at Glu299 is shown, and peaks corresponding to the detected fragments are annotated. Actx = active site peptide.

5.2.3 Activity-based protein profiling of IDUA in homogenates of fibroblasts

It was attempted to use ABP **2** to visualize endogenous IDUA in lysates of cultured normal human dermal fibroblasts (NHDF) and concentrated human urine, with and without

ABPs for α-L-iduronidase

pre-purification by concanavalin A beads. Unfortunately, no clear labeling on rIDUA was observed with ABP 2 at 1–10 μM concentration, and many non-specific bands were detected at higher concentrations, that could not be competed by inhibitor 1 nor ABP 3 (data not shown). To investigate whether the lack of specific IDUA labeling in NHDF lysates is due to low enzyme amount, the specific glycosidase activity and ABP labeling of IDUA vs. β-glucocerebrosidase (GBA) with those of the corresponding Cy5 ABPs (2 vs. ABP JJB367²¹) was compared in recombinant enzymes and NHDF lysates. It was observed that while it is theoretically possible to detect IDUA in fibroblast lysates (calculated amount of IDUA in lysates was only 1.5 lower than that of GBA in the same lysates), its detection in NHDF lysates is still challenging due to nonspecific labeling of other proteins at the required concentration of ABP 2 (25–50 μM) (Fig. 5.6). On the other hand, measurement of ABP 2’s inhibition on IDUA in NHDF lysates showed

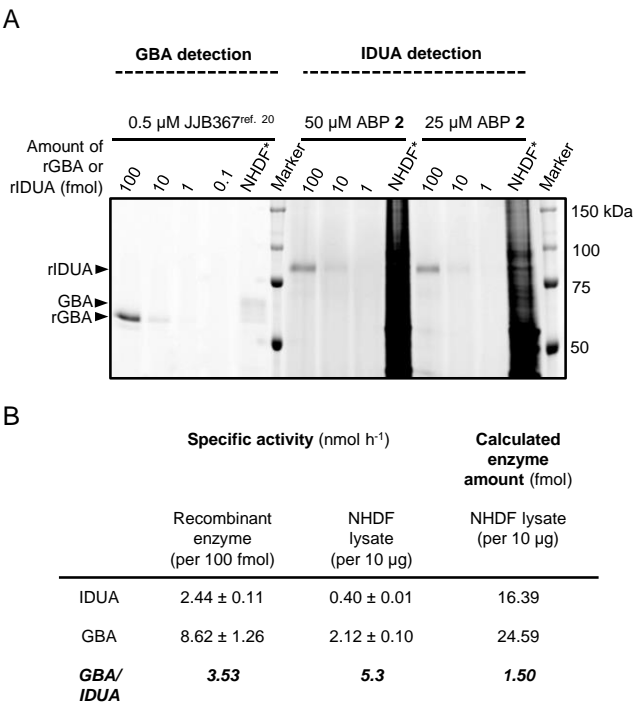


Figure 5.6. Detection of endogenous IDUA in human fibroblasts (NHDF) lysates. A) Comparing endogenous enzyme amount in human fibroblasts (NHDF) lysates for IDUA vs glucocerebrosidase (GBA), by comparing measured specific activity presented in lysates vs from known amount of rIDUA or rGBA with 4-methylumbelliferyl-glycoside substrates. B) Comparing ABP labeling of known amounts of rGBA and rIDUA vs ABP labeling in NHDF lysates. *10 μg protein was loaded.

an apparent IC_{50} value of 23.5 μ M (**Fig. 5.S5**), comparable to the value towards rIDUA. Therefore, it was concluded that direct detection of IDUA in biological samples by ABP **2** via SDS-PAGE is not feasible due to a combination of this compound's moderate activity and a lack of relative substrate specificity. Future optimization of enrichment method for endogenous IDUA is warranted for its eventual application in diagnostic purposes.

5.2.4 Conformations of α -L-ido-aziridine **11** and α -L-idoA-aziridine by DFT calculations

The conformational preferences of α -L-ido-aziridine **11** and α -L-idoA methylated aziridine was studied (Department of Bio-organic Synthesis, Leiden University), as simplified representations of inhibitors **1–3**, in order to elucidate the involvement of conformation on inhibitor potency and binding kinetics. A conformer distribution search in Spartan 14²² and further optimization with Gaussian 09²³ by utilizing B3LYP/6–311G(d, p)/PCM(H₂O) (for details, see section 5.S3 in the **Appendix**) showed that the ⁴H₃ conformation of α -L-ido-aziridine **11** is greatly favored, with variations in the geometry about the C5–C7 bond (**Table 5.S2**). Conversely, α -L-idoA-aziridine showed both ⁴H₃ and ³H₄ (the latter 1.4 kcal mol⁻¹ higher in energy) as relevant conformations. Interestingly, the ^{2,5}B boat conformation was also found as a relevant geometry for α -L-idoA-aziridine, albeit with an energetic cost of 8.0 kcal mol⁻¹. In addition, coupling constants (*J*) were calculated for the lowest-energy conformations, and these were in excellent agreement with experimental NMR data (**Table 5.S3, 5.S4**).

5.2.5 Structural analysis of IDUA interactions with inhibitors **1–3**

In order to study the mechanism of action of inhibitors **1–3**, their conformations upon binding to IDUA were analyzed by crystallographic studies by collaboration with the Gloster group (University of St Andrews). Compounds were applied in solution for various durations to raIDUA crystals (IDUA recombinantly expressed in the seeds of a cgl (complex glycan deficient) mutant of *Arabidopsis thaliana*). Data were collected from a crystal soaked with ABP **1** for 24 h to 2.02 Å resolution (**Table 5.S1**), which revealed the structure of raIDUA in a covalent complex with **1** (**Fig. 5.7A**). The aziridine nitrogen is displaced by nucleophilic attack of the active site carboxylate to form a trans-2-amino ester (with the rest of the R group not visible in the electron

density, presumably disordered due to its inherent flexibility; this region of the structure is exposed to the solvent). Interestingly, the pseudo-glycoside was observed in a $^5\text{S}_1$ skew-boat conformation, which differs slightly from the distorted ^2_5B boat conformation reported for the previously described irreversible inhibitor 2-deoxy-2-fluoro- α -L-ido-pyranosyluronic acid

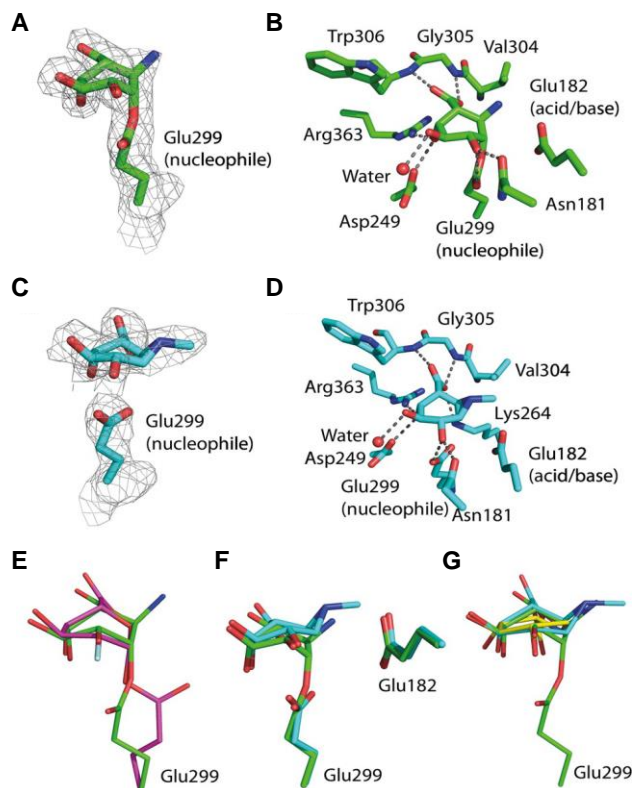


Figure 5.7. Structural insights into ralDUA complexed with ABPs. A) Structure of ralDUA complexed with a fragment of compound **1**, which is covalently linked to the nucleophile Glu299. The maximum likelihood/ s_A weighted $2F_{\text{obs}} - F_{\text{calc}}$ electron density map (gray) is contoured at 1.2 sigma. B) Structure of ralDUA covalently complexed with a fragment of compound **1**, illustrating the active site residues that interact with the pseudo-glycoside. C) Structure of ralDUA complexed with a fragment of ABP **3**. The nucleophile Glu299 is shown. The maximum likelihood/ s_A weighted $2F_{\text{obs}} - F_{\text{calc}}$ electron density map (gray) is contoured at 1.0 sigma. D) Structure of ralDUA complexed with a fragment of ABP **3**, illustrating the active site residues that interact with the pseudo-glycoside. E) Superposition of ralDUA covalently complexed with fragments of compound **1** (green) and 2F-IdoA (pink; PDB code 4KH2⁸). F) Superposition (based on alignment of protein main-chain atoms) of ralDUA complexed with a fragment of compound **1** (covalent, green) and a fragment of ABP **3** (transition state, cyan). G) Superposition (based on alignment of C3 and C4 atoms of each molecule) of ralDUA complexed with a fragment of compound **1** (covalent, green), a fragment of ABP **3** (transition state, cyan), and IdoA-DNJ (Michaelis complex, yellow; PDB code 4KGL).⁸

(2F-IdoA) covalently bound to IDUA.⁸ The observed 5S_1 conformation of the covalent inhibitor **1**–enzyme complex supports predictions for the conformational itinerary followed by α -L-iduronidase GH39 (**Fig. 5.1A**).⁷ The carboxylate group of the pseudo-iduronic acid forms bidentate hydrogen bonds with the main-chain nitrogen atoms of Gly305 and Trp306, the C4 hydroxyl group forms hydrogen bonds with Arg363 and Asp349, the C3 hydroxyl group interacts with Asp349 and a water molecule, and the C2 hydroxyl group forms hydrogen bonds with Asn181 and the nucleophile Glu299 (**Fig. 5.7B**). In the covalent complex between IDUA and 2F-IdoA, the nucleophile Glu299 is rotated by around 90 °C compared to the position observed in the complex here with the fragment of **1**,⁸ and the fluoro group at C2 may preclude an interaction with O ϵ 2 of Glu299, causing it to rotate. However, the inhibitor **1**–IDUA complex presented here, bearing a hydroxyl group at C2 and showing an interaction with Glu299, is more likely to represent what occurs during catalysis (**Fig. 5.7E**).

In an attempt to fully define the conformational inhibition of compounds **1–3**, raIDUA crystals were soaked with the ABPs for shorter durations. Data collected to 2.39 Å resolution (**Table 5.S1**) on a crystal soaked with ABP **3** for 45 min revealed electron density in the active site of raIDUA consistent with the unreacted cyclophellitol aziridine **3** (**Fig. 5.7C**). A methyl group on the cyclophellitol aziridine was visible, but the rest of the R group was not evident and presumably disordered. Interestingly, the pseudo-glycoside was observed in a 2_5B conformation, which is the predicted transition state for GH39 α -L-iduronidase.⁷ The majority of the interactions with active-site residues were the same as those described for the covalent complex with raIDUA (**Fig. 5.7D**), although a shift in position of the glycoside indicated that the carboxylate group additionally interacted with Lys264. The hydroxyl group at C2 forms a hydrogen bond with the nucleophile O ϵ 2 of Glu299, but at a surprisingly short distance of 2.4 Å, suggesting a tight interaction. This close proximity results in a distance between the pseudo-anomeric carbon and O ϵ 1 of only 2.9 Å. These tight interactions, together with the 2_5B conformation of the pseudo-glycoside, suggest that the pseudo-glycoside at the transition state was being observed; such structural observations are rare using wild-type enzymes, but here it was possible due to the slow inactivation kinetics of **3**. The importance of the interaction

between the glycoside and the C2 hydroxyl group supports work by others;^{24, 25} indeed, interactions at the 2-position were estimated to contribute 18 kJ mol⁻¹ binding energy to stabilization of the transition state for a β -glucosidase during the glycosylation step of the catalysis.²⁴ Based on this work, it was postulated that a hydrogen bond formed between the C2 hydroxyl group and the nucleophile would be optimal at the transition state, as the two groups come into close proximity during formation of the covalent glycosyl–enzyme bond.²⁴

Superimposition of the main chain atoms for the two complexes revealed a shift in the position of the cyclophellitol aziridine to accommodate formation of the covalent bond (**Fig. 5.7F**). This engendered movement of between 0.2 and 0.4 Å at C5, C4 and C3, 0.5 Å at C2, 0.6 Å at the carbon at the position of the endocyclic oxygen, and 1.1 Å at the pseudo-anomeric carbon. These structures, together with the previously reported structure of IDUA in complex with the inhibitor IdoA-DNJ, in which the pseudo-glycoside was observed in a ²S₀ conformation (predicted Michaelis complex conformation), allows the full conformational itinerary for IDUA to be structurally defined. The structures of IDUA with IdoADNJ (Michaelis complex) and **3** (transition state complex) and the fragment of compound **1** (covalent complex) were overlapped at the C3 and C4 atoms (**Fig. 5.7G**). This clearly shows the electrophilic migration from the Michaelis complex in a ²S₀ conformation, through the transition state in a ²⁵B conformation, to the covalent intermediate in a ⁵S₁ conformation. At the pseudo-anomeric carbon, there is a displacement of 0.74 Å from the Michaelis complex to the covalent intermediate. This is accompanied by a small (0.23 Å) movement at C2, but larger movement at C5 (0.72 Å) and the atom at the position of the endocyclic oxygen (0.70 Å), presumably to bring about the required migration at the anomeric position.

5.2.6 Visualizing rIDUA uptake in normal and patient cells

Finally, the question whether ABP **2** could be used to study rIDUA cellular uptake and lysosomal internalization was investigated. The majority of therapeutic glycosidases are amended with mannose 6-phosphate (M6P) residues for their recognition by M6P receptors (MPRs) on the plasma membrane and consequent transport to the lysosomes. In order to track the rIDUA

within cells, NHDF and fibroblasts of MPS I and ML II patients were fed with pre-labeled rIDUA-ABP **2**, and after fixation, cells were analyzed by confocal fluorescence microscopy. After 16 h incubation, punctate fluorescence structures were observed, which colocalized with the signals from the antibody-labeled lysosomal-associated membrane protein 1 (LAMP1), indicating lysosomal uptake of labeled rIDUA by all analyzed fibroblast models (**Fig. 5.8A**). The fluorescence from labeled rIDUA was absent in cells without the addition of rIDUA, as well as cells pre-incubated with M6P, which blocks M6P receptors (**Fig. 5.8A**). This finding was recapitulated in a parallel experiment, in which identically treated cells were lysed and detected for Cy5 fluorescence by SDS-PAGE and fluorescent scanning, revealing that only cells treated with ABP **2**-labeled rIDUA and without M6P pre-incubation contained bands corresponding to rIDUA (**Fig. 5.8B**). Interestingly, two extra bands that were smaller than the original rIDUA (85 kDa) were observed in the NHDF lysates, whereas only one band of 74 kDa and one band of 85 kDa was observed in lysates of MPS I or ML II fibroblasts, respectively. The 74 kDa and lower molecular bands were possibly rIDUA processed in the lysosomes of NHDF,²⁶ and this difference in labeling patterns could therefore indicate difference in the lysosomal function or endosomal uptake between normal and patient cells. Altogether, these results clearly demonstrated that rIDUA lysosomal uptake is mediated by MPRs, in agreement with earlier literature,²⁷ and that ABP **2** can be used to study the trafficking, localization, and lysosomal processing of rIDUA within cells derived from MPSI and MLII patients.

5.3 Discussion

In this chapter, the characterization and application of newly synthesized α -L-iduronidase inhibitors and ABPs were discussed. α -L-ido-configured cyclophellitol aziridine was synthesized as a key intermediate for generation of the first α -L-iduronidase ABPs. The α -L-ido-configured cyclohexene **8** could be an interesting starting point for the development of new IDUA inhibitors or chaperones. With the inhibitors described herein, ABPP studies on rIDUA has been conducted, showing that ABP **2** irreversibly labels rIDUA in a concentration- and time-dependent manner, with optimum labeling at pH 4.5–5.0. The covalent rIDUA inhibition has been further demonstrated by nano-LC-MS/MS, detecting a 7-amino-acid peptide fragment of

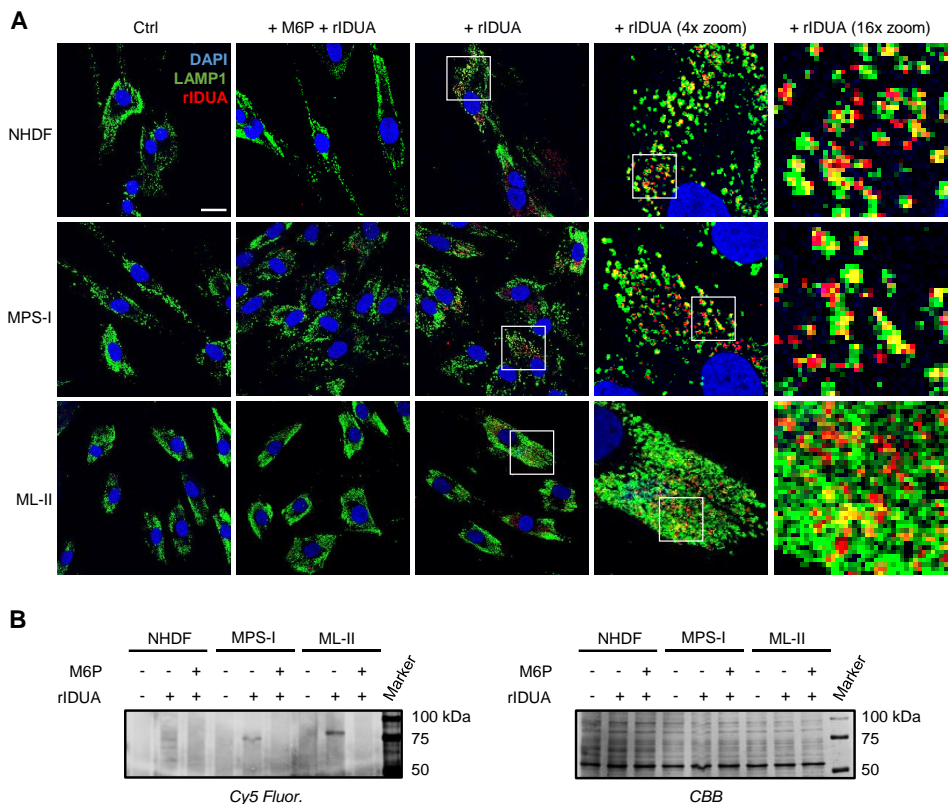


Figure 5.8. rIDUA visualization in human fibroblasts by confocal fluorescence microscopy and SDS-PAGE. A) From top to bottom: NHDF, human normal dermal fibroblasts; MPS I, patient fibroblasts with mucopolysaccharidosis type I, and ML II, patient fibroblasts with mucopolipidosis type II. From left to right: cells were incubated without (Ctrl) or with ABP 2-prelabeled rIDUA (+rIDUA, with successive zoomed-in images from areas within the indicated white squares), or pre-treated with man-nose-6-phosphate prior to rIDUA incubation (+M6P +rIDUA). Color legend: nuclei were stained with DAPI (blue), lysosomes with immunostaining of lysosomal-associated membrane protein 1 (LAMP1) (green), and rIDUA was labeled with ABP 2 (red). Scale bar =25 mm. B) Lysates of cells with identical treatment, detected for Cy5 fluorescence by fluorescent scanning on the wet slab gel, after samples were resolved by SDS-PAGE (left panel) The same gel was stained for Coomassie Brilliant Blue (CBB) for analysis of protein loading amount (right panel).

rIDUA containing the nucleophilic residue bound to ABP 3.

It was found that the α -L-iduronidase inhibitors and ABPs exhibited much lower inhibitory potency and slower binding kinetics compared to earlier generated cyclophellitol aziridines conformers, such as the β -gluco-aziridine ABP JJB367 for GBA²⁰. This was explained by DFT

calculations, which showed that inhibitors **1–3** adopt mainly a half-chair conformation ($^4\text{H}_3$ and $^3\text{H}_4$) in solution, with the $^2, ^5\text{B}$ conformation also as relevant geometry at an extra cost of 8.0 kcal mol⁻¹. Furthermore, crystallographic studies showed that compounds **1–3** bind IDUA in a $^2, ^5\text{B}$ boat conformation in the Michaelis complex. As a consequence, the half-chair conformations ($^4\text{H}_3$ and $^3\text{H}_4$) of inhibitors **1–3**, as predicted by DFT calculations, differ from any of the reaction itinerary conformations of α -L-iduronidase depicted in **Fig. 5.1A**, and thus inhibitors **1–3** may need to overcome this 8.0 kcal mol⁻¹ energetic barrier to adopt the Michaelis complex transition state ($^2, ^5\text{B}$) conformation. Therefore, it is likely that the lower potency and slower inhibition kinetics of α -L-idoA-aziridine analogues on rIDUA is a manifestation of this energetic barrier.

Structural evidence for covalent addition of the ABPs to the nucleophilic residue of rIDUA was also provided by crystallographic studies. In the process, the conformation of the cyclophellitol aziridine at the transition state and in the covalent intermediate was defined, which supports earlier predictions concerning the conformational itinerary followed by α -L-iduronidase.⁷ The insights gained through these studies should help in the design of closer conformational $^2, ^5\text{B}$ analogues by the use of different electrophilic traps or reactive species for the generation of improved inhibitors or molecular chaperones, with the end goal being the future provision of improved therapies for MPS I patients.

IDUA labeling with ABP **2** in complex biological samples—such as cell lysates, was not successful due to lower potency and lack of relative selectivity of this analogue at the applied concentration (low μM) compared with previously reported glycosidase probes. Future optimization on ABP labeling conditions and IDUA purification procedures from the desired sample are warranted, in order to utilize the ABPs for studying endogenous IDUA from clinical or laboratory samples. On the other hand, it was demonstrated that ABP **2** can be used to study the localization and trafficking of therapeutic rIDUA within cultured cells. It was shown that the rIDUA–ABP **2** complex is recognized by MPRs and internalized in lysosomes, and possibly processed differently between normal and patient fibroblasts.

5.4 Experimental procedures

5.4.1 Materials

Recombinant human iduronidase (rIDUA) was obtained from Genzyme (Aldurazyme®). Normal human dermal fibroblasts (NHDF) were obtained from Lonza. Human patient fibroblasts (MPS-I and ML-II) were obtained with consent from donors from the Academic Medical Center in Amsterdam, the Netherlands. 4-methylumbelliferyl α -L-iduronide (4-MU- α -L-IdoA) was purchased from Glycosynth. Pierce™ Bicinchoninic acid (BCA) protein assay kit and Pierce™ Polyacrylamide Spin Desalting Columns 7K MWCO was acquired from Thermo Fisher Scientific. All other chemicals were obtained from commercial sources.

5.4.2 Cell culture and lysate preparation

Fibroblasts were cultured in Dulbecco's modified Eagle's medium: Nutrient Mixture F-12 (DMEM/F-12, Invitrogen), containing 10 % (v/v) heat-inactivated fetal calf serum, 200 μ g/mL penicillin, 200 μ g/mL streptomycin, at 37 °C and 5 % CO₂. Confluent Fibroblasts were subcultured at a ratio of 1:4 each week. To prepare lysates, cells were washed three times with phosphate-buffered saline (PBS), detached by scraping in the presence of ice-cold lysis buffer (25 mM K₂HPO₄/KH₂PO₄ pH 6.5, supplemented with 0.1 % (v/v) Triton X-100 and protease inhibitor cocktail tablet (Roche ,version 12)), and collected in Eppendorf tubes. The collected suspension was vortexed vigorously, incubated on ice for 1 h, freeze-thawed once using liquid nitrogen, and stored at -80 °C. Concentration of lysates was determined using BCA kit.

5.4.3 Iduronidase activity assay using 4-MU- α -L-IdoA as substrate

Samples containing enzyme were diluted in assay buffer (150 mM citrate/Na₂HPO₄, pH 4.5, supplemented with 0.1 % (v/v) Triton X-100, 0.15 M NaCl, 33 mM CaCl₂, 33 mM MgCl₂), and load onto a black flat-bottom 96-well plate (Greiner) in triplicates of 25 μ L per well. Negative controls (blank) were prepared by substituting enzyme samples with buffer. For reaction, samples were added with 25 μ L of 360 μ M 4-MU- α -L-IdoA²⁸ (prepared in assay buffer supplemented with 0.1 % (w/v) bovine serum albumin (BSA)), and incubated at 37 °C for 30

min to 4h. Reaction was stopped by adding 200 μL 1 M Glycine-NaOH (pH 10.3), and fluorescence was measured using a LS-55 fluorometer (PerkinElmer) at $\lambda_{\text{ex}} = 366 \text{ nm}$ and $\lambda_{\text{em}} = 445 \text{ nm}$.

5.4.4 Apparent IC_{50} values of inhibitors and ABPs on recombinant human iduronidase and cell lysates

Inhibitors and ABPs were diluted at various concentrations in 12.5 μL assay buffer and incubated with 12.5 μL rIDUA (5.8 ng, or 70 fmol) or fibroblast lysates (50 μg protein), both diluted in assay buffer, at 37°C for 1 h (rIDUA) or 4 h (fibroblasts lysates), at 1 % (v/v) DMSO concentration. This was followed by iduronidase activity assay (30 min incubation time) described in the previous section. The detected 4-MU fluorescence at each concentration for each compound were normalized to the fluorescence from the control sample without inhibitor, and data were fitted with [inhibitor] *vs* response – variable slope (four parameters) function in GraphPad Prism 7.0 software to obtain apparent IC_{50} values.

5.4.5 Labeling and SDS-PAGE of recombinant human iduronidase

To prepare for labeling, rIDUA stock (0.58 $\mu\text{g}/\mu\text{L}$ in PBS) was diluted with assay buffer to final concentration of 10 ng (120 fmol) in 14 μL assay buffer, if not otherwise specified. ABP **2** stock (15 mM in DMSO) was diluted subsequently with DMSO and then assay buffer, to 8x of intended assay concentration obtaining 4 % (v/v) DMSO. For labeling, 2 μL of ABP **2** dilution was incubated with 14 μL enzyme dilution at 37 °C for the intended time periods. Labeling was terminated by denaturing samples with 4 μL sample buffer (5x Laemmli buffer, containing 0.3 M Tris-HCl pH 6.8, 50 % (v/v) 100 % glycerol, 8 % (w/v) dithiothreitol (DTT), 10 % (w/v) sodium dodecyl sulfate (SDS), 0.01 % (w/v) bromophenol blue) and heated at 98 °C for 5 minutes. SDS-PAGE and fluorescence detection procedures followed the previously described methods.²¹

5.4.6 Labeling of recombinant human iduronidase at different pH

Assay buffers with pH 2.5–8.0 were used to dilute rIDUA and ABP **2**. The experiment was

ABPs for α -L-iduronidase

performed with 10 ng rIDUA at 10 μ M ABP **2** (assay concentration) in 16 μ L volume and 1 h incubation time, followed by denaturation, SDS-PAGE, and fluorescence scan.

5.4.7 Reversibility of labeling of ABP **2** on recombinant human iduronidase

5 μ L rIDUA stock (0.58 μ g/ μ L in PBS) was diluted with 20 μ L assay buffer without Triton X-100, and incubated with either 25 μ L ABP **2** (150 μ M and 1 % (v/v) DMSO) or 25 μ L assay buffer containing 0.1 % (w/v) DMSO for 1 h at 37 °C. Thereafter, 45 μ L of sample was passed through a desalting column, and diluted with 216 μ L assay buffer (with Triton X-100) to a final enzyme concentration of 1 ng/ μ L. For assessing the reversibility of labeling/inactivation of ABP **2** on rIDUA, both samples were kept at 4 °C until subjecting to iduronidase activity assay using 4-MU- α -IdoA at the following time points after desalting: 0.5, 28, and 100 h. Iduronidase activity assay was performed with 1 μ L sample in triplicates, and assay buffer was used as blank.

5.4.8 Competitive ABPP experiments

For the competitive ABPP (cABPP) experiment using 4-MU- α -IdoA as an active-site directed inhibitor, 10 ng rIDUA, or no-enzyme blank (PBS), was prepared in 7 μ L assay buffer (pH 4.5). This was pre-incubated with 7 μ L assay buffer containing 4-MU- α -IdoA (0.2–20 mM) on ice for 5 min, then incubated with 1 μ L ABP **2** (750 μ M, 8 % (v/v) in assay buffer) or DMSO control (8 % (v/v) in assay buffer) at 37 °C for 2 h. In the same experiment, 7 μ L SDS (4 % (w/v)) was added to the 7 μ L enzyme, pre-incubated at 98 °C for 2 min, and incubated with ABP **2** at 37 °C for 2 h. For the cABPP experiment with compound **1**, 10 ng rIDUA was prepared in 12 μ L assay buffer, pre-incubated with 2 μ L compound **1** (2.8 mM – 70 μ M, 18.6% DMSO in assay buffer) at 37 °C for 2 h, then incubated with 2 μ L ABP **2** (100 μ M, 4 % DMSO in assay buffer) at 37 °C for 2 h. Samples were then denatured, and subjected to SDS-PAGE and fluorescence scan.

5.4.9 Kinetic parameters of ABP **2**

The kinetic parameters of ABP **2** for rIDUA was determined by an SDS-PAGE-based assay, in which the intensity of fluorescent signal from ABP **2**-labeled rIDUA on the wet slab gel is proportional to the extent of rIDUA inactivation, which was normalized to the signal from a

control group with saturate labeled rIDUA. rIDUA was labeled with ABP **2** for different time periods and at different ABP **2** concentrations (which were \gg enzyme concentration), and the kinetic parameters k_{inact} (pseudo first-order inactivation rate constant) and K_I (inhibition constant) were obtained using non-linear curve fitting. To perform the experiment, three sets of rIDUA were diluted in series of 1.5 mL Eppendorf tubes to 10 ng (120 fmol) per 14 μ L, and labeled with 2 μ L ABP **2** (diluted in DMSO and assay buffer to various concentrations and [DMSO] fixed at 8 % (v/v)) for 30, 60, 90, 120, or 150 min. Concentrations in assay were 5 μ M, 10 μ M, 20 μ M, 30 μ M, 40 μ M, 50 μ M, or 60 μ M for ABP **2**, 7.5 nM for rIDUA, and 1 % (v/v) for DMSO. Reaction was terminated by incubating samples with sample buffer at 98°C for 5 min. Samples were subjected to SDS-PAGE and fluorescence scan, and Cy5 fluorescence from the ABP **2**-labeled rIDUA was quantified using ImageQuant software (GE Healthcare). The incubation condition for maximum labeling (complete inactivation) on rIDUA for ABP **2** was determined to be 60 μ M and 150 min, and a control sample with this condition was loaded on every gel to allow normalization of signals from samples in the same gel. After normalization, the value at each ABP **2** concentration were plotted in a time vs % labeling (inactivation) graph, and the plotted data were fitted with one-phase exponential association function to obtain the rate constant k at each ABP **2** concentration. Finally, in a second plot the obtained k values were plotted against ABP **2** concentrations, and the data were fitted with a Michaelis-Menten equation to obtain k_{inact} and K_I values for ABP **2** on rIDUA for each set ($n = 3$). All non-linear curve-fitting was performed using GraphPad Prism 7.0 software.

5.4.10 LC-MS/MS identification of rIDUA active site peptide

A total of 10 μ g rIDUA was diluted in assay buffer and incubated with either 75 μ M ABP **3** or DMSO (negative control) for 1 h at 37 °C in 100 μ L volume ([DMSO] = 0.5 % (v/v)). The samples were then added with 100 μ g BSA (100 μ L), and followed by chloroform/methanol precipitation and reduction/alkylation procedures described previously.²⁹ Consequently, the samples were dissolved in 2 % (w/v) SDS and diluted with 50 mM Tris-HCl (pH 7.8) to a final SDS concentration of 0.05 % (w/v). The samples were then concentrated with size exclusion columns (Amicon 10 k) to a volume of 74 μ L, and digested O/N at 25 °C with 1.1 μ g

ABPs for α -L-iduronidase

Chymotrypsin (Promega) in the presence of 10 mM CaCl₂. Digested peptides were pulled-down using 50 μ L of Streptavidin paramagnetic beads (MyOne T1, ThermoFisher) in 1 mL of pull-down buffer (50 mM Tris-HCl (pH 7.5), 150 mM NaCl, 0.5 % (w/v) SDS) for 1 h at RT under vigorous shaking. The beads were washed stringently following previously described procedures²⁹ and eluted with 100 μ L of elution buffer (25 % (v/v) acetonitrile, 5 % (v/v) formic acid, 70 H₂O, 10 μ M biotin) for 30 min at 37°C. Afterwards, acetonitrile in the supernatant were evaporated using a Speedvac at 45°C, and this was followed by desalting using StageTips. The eluate was evaporated and reconstituted in 20 μ L of LC-MS sample solution (95: 3: 0.1, H₂O: acetonitrile: formic acid) for LC-MS/MS analysis. Peptide samples were analyzed with a two-hour gradient of 5 % to 25 % acetonitrile on nano-LC, hyphenated to an LTQ Orbitrap and identified by manual search for the theoretical m/z values of the active site peptide and its MS/MS fragments labeled with ABP 3.

5.4.11 Comparing specific activity and ABP labeling between GBA and IDUA

For measurement of GBA activity, 100 fmol of rGBA (Cerezyme/Imiglucerase, Genzyme) or NHDF lysates (10 μ g protein) were diluted in 25 μ L of GBA buffer (150 mM citric acid/Na₂HPO₄, 0.1 % (v/v) Triton X-100, 0.2 % (w/v) sodium taurocholate) and incubated with 100 μ L GBA substrate mixture (3.75 mM 4-MU- β -D-glucopyranoside (Glycosynth), in GBA buffer, 0.1 % (w/v) BSA) for 30 min at 37 °C. IDUA activity was measured following the methods described in previous section. For ABP labeling of GBA, rGBA (100 – 0.1 fmol) or NHDF lysates (10 μ g protein) were diluted in 14 μ L GBA buffer, and incubated with 0.5 μ M JJB367²¹ for 30 min at 37 °C ([DMSO] = 0.5 (v/v)). For ABP labeling of IDUA, rIDUA (1–100 fmol) or NHDF lysates (10 μ g protein) were diluted in 14 μ L assay buffer and incubated with either 50 μ M or 25 μ M ABP 2 for 4 h at 37 °C ([DMSO] = 0.5 % (v/v)). Samples were denatured, and proceeded to SDS-PAGE and fluorescent detection.

5.4.12 Recombinant expression and purification of IDUA in seeds of *Arabidopsis thaliana* (University of St Andrews)

Recombinant human α -L-iduronidase (abbreviated to raIDUA to distinguish from rIDUA

obtained from Genzyme) was produced in seeds of *Arabidopsis thaliana cgl* (complex *glycan* deficient) line A4.7³⁰ in which the seeds (T3 generation) accumulated raIDUA to 7.2 ± 0.6 % total soluble protein (9.8 $\mu\text{g}/\text{mg}$ dry seeds). raIDUA was purified to homogeneity from the T3 seeds using concanavalin A-sepharose and anti-IDUA affinity chromatography as described previously^{31, 32}. In human IDUA, there are six N-linked glycosylation sites. The oligosaccharide structures at each site of rIDUA secreted from a Chinese hamster ovary (CHO) cell line have been determined by mass spectrometry³³. The raIDUA expressed in the seeds of the *cgl* mutant of *Arabidopsis* has much reduced complexity in these N-linked glycans, the majority of which are non-matured, high mannose N-glycans^{30, 34}.

5.4.13 Crystallization of raIDUA (University of St Andrews)

raIDUA was further purified by size exclusion chromatography using an S200 10/300 column (GE Healthcare) equilibrated in 20 mM Tris, pH 7.0, 500 mM NaCl, and 0.02 % sodium azide. The fractions containing raIDUA were buffer exchanged using a PD10 desalt column (GE Healthcare) into 20 mM dimethylglutaric acid, pH 6.0, 0.2 M NaCl, 5 % (v/v) glycerol, and 5 % (v/v) ethanol and concentrated to 10 mg/ml for crystallization. Crystallization was performed in a 24 well plate using hanging-drop vapor diffusion. The rhomboid-plate shaped crystals grew at room temperature from 0.1 M HEPES, pH 7.5, 0.26 M sodium potassium tartrate, 20 % (w/v) polyethylene glycol 3350 (optimized from the crystallization condition reported by Bie *et al.*⁸). Crystals were soaked in mother liquor containing a minute amount of solid **1** for 24 hours or **3** for 45 minutes, before being harvested. Crystals were cryo-protected in a solution containing the mother liquor plus 30 % glycerol prior to vitrification in liquid nitrogen.

5.4.14 Data collection and processing for raIDUA crystals (University of St Andrews)

X-ray diffraction data were collected at Diamond Light Source (DLS) on beamlines I03 and I04; the data processing and refinement statistics can be found in **Table 4.S1**. Diffraction data were processed either using the FastDP pipeline³⁵ (which utilizes XDS³⁶ with Aimless³⁷) or Xia2³⁸ (also with XDS³⁶ with Aimless³⁷). Molecular replacement was performed using Phaser³⁹ with Protein Data Bank (PDB) entry 4JXO as the search model. Refinement was performed using

ABPs for α -L-iduronidase

REFMAC5⁴⁰ and manual model building was done using Coot⁴¹. Structures were validated using PDB_REDO⁴². Models for the fragments of **1** and **3** were built in JSME⁴³ and the libraries generated with PRODRG⁴⁴.

5.4.15 Fibroblasts uptake of ABP **2**-labeled rIDUA

rIDUA was diluted to 58 ng/ μ L and labeled with ABP **2** at 75 μ M for 1 h at 37 °C in a volume of 40 μ L. After incubation, unbound ABP **2** in solution was removed by passing through desalting columns (Pierce™ Polyacrylamide Spin Desalting Columns 7K MWCO), and the eluate were diluted in assay buffer without Triton X-100, to a final rIDUA concentration of 10 ng/ μ L. For the uptake experiment, human normal and patient fibroblasts were sub-cultured 1 day before treatment in 12-well plates (1 mL culture medium per well) with or without glass coverslips. Cells were then pre-treated with 4 mM mannose-6-phosphate (M6P, diluted in water) or same volume of water for 1 h, followed by treating with ABP **2**-labeled rIDUA (100 ng/mL culture medium) for 20 h, without removing M6P. A control group was included for each cell type, treated only with water and assay buffer. Confocal microscopy analysis was carried out following a previously described procedure⁴⁵, where samples were fixed with 4 % formaldehyde, permeabilized with 0.1 % (w/v) saponin and 2 % (w/v) BSA, and immuno-stained for the lysosomal membrane protein LAMP1 using mouse anti human LAMP1 (Southern Biotech) as primary antibody, and donkey anti mouse Alexa488 (Molecular Probes) as secondary antibody. The coverslips were mounted to microscopy slides using ProLong™ Diamond Antifade Mountant with DAPI (Thermo Fisher), and scanned using a Leica SP8 confocal microscope for DAPI, Alexa488, and Cy5 fluorescence with a 40x oil-immersed objective. Pictures at each fluorescence channel were captured at 1024 x 1024 resolution, with $n = 3$ frame averages.

5.5 References

- 1 Lombard V, Golaconda Ramulu H, Drula E, Coutinho PM & Henrissat B (2014) The carbohydrate-active enzymes database (CAZy) in 2013. *Nucleic Acids Res* **42**, D490–495.
- 2 Nieman CE, Wong AW, He S, Clarke L, Hopwood JJ & Withers SG (2003) Family 39 alpha-L-iduronidases and beta-D-xylosidases react through similar glycosyl-enzyme intermediates: identification of the human iduronidase nucleophile. *Biochemistry* **42**, 8054–8065.
- 3 Archer LD, Langford-Smith KJ, Bigger BW & Fildes JE (2014) Mucopolysaccharide diseases: a complex interplay between neuroinflammation, microglial activation and adaptive immunity. *J Inher Metab Dis* **37**, 1–12.
- 4 Clarke LA (2008) The mucopolysaccharidoses: a success of molecular medicine. *Expert Rev Mol Med* **10**, e1.
- 5 Maita N, Tsukimura T, Taniguchi T, Saito S, Ohno K, Taniguchi H & Sakuraba H (2013) Human α -L-iduronidase uses its own N-glycan as a substrate-binding and catalytic module. *Proc Natl Acad Sci U S A* **110**, 14628–14633.
- 6 Koshland DE (1953) Stereochemistry and the mechanism of enzymatic reactions. *Biol Rev* **28**, 416–436.
- 7 Speciale G, Thompson AJ, Davies GJ & Williams SJ (2014) Dissecting conformational contributions to glycosidase catalysis and inhibition. *Curr Opin Struct Biol* **28**, 1–13.
- 8 Bie H, Yin J, He X, Kermod AR, Goddard-Borger ED, Withers SG & James MN (2013) Insights into mucopolysaccharidosis I from the structure and action of α -L-iduronidase. *Nat Chem Biol* **9**, 739–745.
- 9 Grewal SS, Wynn R, Abdenur JE, Burton BK, Gharib M, Haase C, Hayashi RJ, Shenoy S, Sillence D, Tiller GE, Dudek ME, van Royen-Kerkhof A, Wraith JE, Woodard P, Young GA, Wulffraat N, Whitley CB & Peters C (2005) Safety and efficacy of enzyme replacement therapy in combination with hematopoietic stem cell transplantation in Hurler syndrome. *Genet Med* **7**, 143–146.
- 10 Clarke LA (1993) Mucopolysaccharidosis Type I. *GeneReviews*. Seattle, WA: University of Washington.
- 11 Coutinho MF, Prata MJ & Alves S (2012) Mannose-6-phosphate pathway: a review on its role in lysosomal function and dysfunction. *Mol Genet Metab* **105**, 542–550.
- 12 Harrak Y, Barra CM, Delgado A, Castaño AR & Llebaria A (2011) Galacto-configured aminocyclitol phytoceramides are potent in vivo invariant natural killer T cell stimulators. *J Am Chem Soc* **133**, 12079–12084.
- 13 Jiang J, Kallemijn WW, Wright DW, van den Nieuwendijk AMCH, Rohde VC, Folch EC, van den Elst H, Florea BI, Scheij S, Donker-Koopman WE, Verhoek M, Li N, Schürmann M, Mink D, Boot RG, Codée JDC, van der Marel GA, Davies GJ, Aerts JMFG & Overkleeft HS (2015) In vitro and in vivo comparative and competitive activity-based protein profiling of GH29 α -L-fucosidases. *Chem Sci* **6**, 2782–2789.
- 14 Clements PR, Brooks DA, Saccone GT & Hopwood JJ (1985) Human alpha-L-iduronidase. 1. Purification, monoclonal antibody production, native and subunit molecular mass. *Eur J Biochem* **152**, 21–28.
- 15 Schuchman EH, Guzman NA, Takada G & Desnick RJ (1984) Human alpha-L-iduronidase. II. Comparative biochemical and immunologic properties of the purified low and high uptake forms. *Enzyme* **31**, 166–175.
- 16 Wu L, Jiang J, Jin Y, Kallemijn WW, Kuo C-L, Artola M, Dai W, van Elk C, van Eijk M, van der Marel GA, Codee JDC, Florea BI, Aerts JMFG, Overkleeft HS & Davies GJ (2017) Activity-based probes for functional interrogation of retaining [beta]-glucuronidases. *Nat Chem Biol* **13**, 867–873.
- 17 Witte MD, Kallemijn WW, Aten J, Li KY, Strijland A, Donker-Koopman WE, Van Den Nieuwendijk AMCH, Bleijlevens B, Kramer G, Florea BI, Hooibrink B, Hollak CEM, Ottenhoff R, Boot RG, Van Der Marel GA, Overkleeft HS & Aerts JMFG (2010) Ultrasensitive in situ visualization of active glucocerebrosidase molecules. *Nat Chem Biol* **6**, 907–913.
- 18 Kallemijn WW, Li KY, Witte MD, Marques ARA, Aten J, Scheij S, Jiang J, Willems LI, Voorn-Brouwer TM, Van Roomen CPAA, Ottenhoff R, Boot RG, Van Den Elst H, Walvoort MTC, Florea BI, Codée JDC, Van Der Marel GA, Aerts JMFG & Overkleeft HS (2012) Novel activity-based probes for broad-spectrum profiling of retaining β -exoglucosidases in situ and in vivo. *Angew Chemie - Int Ed* **51**, 12529–12533.
- 19 Jiang J, Kuo CL, Wu L, Franke C, Kallemijn WW, Florea BI, Van Meel E, Van Der Marel GA, Codée JDC, Boot RG, Davies GJ, Overkleeft HS & Aerts JMFG (2016) Detection of active mammalian GH31 α -glucosidases in health and disease using in-class, broad-spectrum activity-based probes. *ACS Cent Sci* **2**, 351–358.
- 20 Willems LI, Beenakker TJ, Murray B, Scheij S, Kallemijn WW, Boot RG, Verhoek M, Donker-Koopman WE, Ferraz MJ, van Rijssel ER, Florea BI, Codée JD, van der Marel GA, Aerts JM & Overkleeft HS (2014) Potent

- and selective activity-based probes for GH27 human retaining α -galactosidases. *J Am Chem Soc* 2014 **136**, 11622–11625.
- 21 Schröder SP, van de Sande JW, Kallemeijn WW, Kuo CL, Artola M, van Rooden EJ, Jiang J, Beenakker TJM, Florea BI, Offen WA, Davies GJ, Minnaard AJ, Aerts JMF, Codée JDC, van der Marel GA & Overkleeft HS (2017) Towards Broad Spectrum Activity-Based Glycosidase Probes: Synthesis and Evaluation of Deoxygenated Cyclophellitol Aziridines. *Chem Commun* **53**, 12528–12531.
 - 22 Shao Y, Molnar LF, Jung Y, Kussmann J, Ochsenfeld C, Brown ST, Gilbert AT, Slipchenko LV, Levchenko SV, O'Neill DP, DiStasio RA Jr, Lochan RC, Wang T, Beran GJ, Besley NA, Herbert JM, Lin CY, Van Voorhis T, Chien SH, Sodt A, Steele RP, Rassolov VA, Maslen PE, Korambath PP, Adamson RD, Austin B, Baker J, Byrd EF, Dachsel H, Doerksen RJ, Dreuw A, Dunietz BD, Dutoi AD, Furlani TR, Gwaltney SR, Heyden A, Hirata S, Hsu CP, Kedziora G, Khallilulin RZ, Klunzinger P, Lee AM, Lee MS, Liang W, Lotan I, Nair N, Peters B, Proynov EI, Pieniazek PA, Rhee YM, Ritchie J, Rosta E, Sherrill CD, Simmonett AC, Subotnik JE, Woodcock HL 3rd, Zhang W, Bell AT, Chakraborty AK, Chipman DM, Keil FJ, Warshel A, Hehre WJ, Schaefer HF 3rd, Kong J, Krylov AI, Gill PM & Head-Gordon M (2006) Advances in methods and algorithms in a modern quantum chemistry program package. *Phys Chem Chem Phys* **8**, 3172–3191.
 - 23 Frisch MJ, Trucks GW, Schlegel HB, Scuseria GE, Robb MA, Cheeseman JR, Scalmani G, Barone V, Men-nucci B, Petersson GA, Nakatsuji H, Caricato M, Li X, Hratchian HP, Izmaylov AF, Bloino J, Zheng G, Sonnenberg JL, Hada M, Ehara M, Toyota K, Fukuda R, Hasegawa J, Ishida M, Nakajima T, Honda Y, Kitao O, Nakai H, Vreven H, Montgomery Jr JA, Peralta JE, Ogliaro F, Bearpark M, Heyd JJ, Brothers E, Kudin KN, Staroverov VN, Ko-bayashi R, Normand J, Raghavachari K, Rendell A, Burant JC, Iyengar SS, Tomasi J, Cossi M, Rega N, Millam JM, Klene M, Knox JE, Cross JB, Bakken V, Adamo C, Jaramillo J, Gomperts R, Stratmann RE, Yazyev O, Austin AJ, Cammi R, Pomelli C, Ochterski JW, Martin RL, Morokuma K, Zakrzewski VG, Voth GA, Salvador P, Dannenberg JJ, Dapprich S, Daniels AD, Farkas O, Foresman JB, Ortiz JV, Cio-slawski J & Fox DJ (2009) Gaussian 09, Revision D.01 [Computer software]. Wallingford CT: Gaussian, Inc.
 - 24 Namchuk MN & Withers SG (1995) Mechanism of Agrobacterium beta-glucosidase: kinetic analysis of the role of noncovalent enzyme/substrate interactions. *Biochemistry* **34**, 16194–16202.
 - 25 Tanaka KSE, Zhu J, Huang XC, Lipari F & Bennet AJ (2000) Glycosidase-catalyzed hydrolysis of 2-deoxyglucopyranosyl pyridinium salts: effect of the 2-OH group on binding and catalysis. *Can J Chem* **78**, 577–582.
 - 26 Unger EG, Durrant J, Anson DS & Hopwood JJ (1994) Recombinant alpha-L-iduronidase: characterization of the purified enzyme and correction of mucopolysaccharidosis type I fibroblasts. *Biochem J* **304**, 43–49.
 - 27 Hasilik A & Neufeld EF (1980) Biosynthesis of lysosomal enzymes in fibroblasts. Synthesis as precursors of higher molecular weight. *J Biol Chem* **255**, 4937–4945.
 - 28 Ou L, Herzog TL, Wilmot CM & Whitley CB (2014) Standardization of alpha-L-iduronidase enzyme assay with Michaelis-Menten kinetics. *Mol. Genet. Metab* **111**, 113–115.
 - 29 Li N, Kuo CL, Paniagua G, van den Elst H, Verdoes M, Willems LI, van der Linden WA, Ruben M, van Genderen E, Gubbens J, van Wezel GP, Overkleeft HS, Florea BI. (2013) Relative quantification of proteasome activity by activity-based protein profiling and LC-MS/MS. *Nat Protoc*, **8**, 1155–1168.
 - 30 He X, Pierce O, Haselhorst T, von Itzstein M, Kolarich D, Packer NH, Gloster TM, Vocadlo DJ, Qian Y, Brooks D & Kermode AR (2013) Characterization and downstream mannose phosphorylation of human recombinant alpha-L-iduronidase produced in Arabidopsis complex glycan-deficient (cgl) seeds. *Plant Biotechnol J* **11**, 1034–1043.
 - 31 He X, Haselhorst T, von Itzstein M, Kolarich D, Packer NH, Gloster TM, Vocadlo DJ, Clarke LA, Qian Y & Kermode AR (2013) Production of alpha-L-iduronidase in maize for the potential treatment of a human lysosomal storage disease. *Nat Commun* **3**, 1062.
 - 32 He X, Haselhorst T, von Itzstein M, Kolarich D, Packer NH & Kermode AR (2012) Influence of an ER-retention signal on the N-glycosylation of recombinant human alpha-L-iduronidase generated in seeds of Arabidopsis. *Plant Mol Biol* **79**, 157–169.
 - 33 Zhao KW, Faull KF, Kakkis ED & Neufeld EF (1997) Carbohydrate structures of recombinant human alpha-L-iduronidase secreted by Chinese hamster ovary cells. *J Biol Chem* **272**, 22758–22765.
 - 34 Pierce OM, McNair GR, He X, Kajura H, Fujiyama K & Kermode AR (2017) N-glycan structures and downstream mannose-phosphorylation of plant recombinant human alpha-L-iduronidase: toward development of enzyme replacement therapy for mucopolysaccharidosis. *Plant Mol Biol* **95**, 593–606.

- 35 Winter G & McAuley KE (2011) Automated data collection for macromolecular crystallography. *Methods* **55**, 81–93.
- 36 Kabsch W (2010) XDS. *Acta Crystallogr D Biol Crystallogr* **66**, 125–132.
- 37 Evans P R & Murshudov GN (2013) How good are my data and what is the resolution? *Acta Crystallogr D Biol Crystallogr* **69**, 1204–1214.
- 38 Winter G. (2010) Xia2: An Expert System for Macromolecular Crystallography Data Reduction. *J. Appl. Crystallogr.* **43**, 186–190.
- 39 McCoy AJ (2007) Solving structures of protein complexes by molecular replacement with Phaser. *Acta Crystallogr D Biol Crystallogr* **63**, 32–41.
- 40 Murshudov GN, Skubak P, Lebedev AA, Pannu NS, Steiner RA, Nicholls RA, Winn MD, Long F & Vagin AA (2011) REFMAC5 for the refinement of macromolecular crystal structures. *Acta Crystallogr D Biol Crystallogr* **67**, 355–367.
- 41 Emsley P, & Cowtan K (2004) Coot: model-building tools for molecular graphics. *Acta Crystallogr D Biol Crystallogr* **60**, 2126–2132.
- 42 Joosten RP, Long F, Murshudov GN & Perrakis A (2014) The PDB_REDO server for macromolecular structure model optimization. *IUCr* **1**, 213–220.
- 43 Bienfait B & Ertl P (2013) JSME: a free molecule editor in JavaScript. *J Cheminform* **5**, 24.
- 44 Schuttelkopf AW & van Aalten DM (2004) PRODRG: a tool for high-throughput crystallography of protein-ligand complexes. *Acta Crystallogr D Biol Crystallogr* **60**, 1355–1363.
- 45 Kuo CL, van Meel E, Kytidou K, Kallemeyn WW, Witte M, Overkleef HS, Artola ME & Aerts JM (2018) Activity-Based Probes for Glycosidases: Profiling and Other Applications. *Methods Enzymol* **598**, 217–235.

APPENDIX

5.S1. Supporting Figures and Tables

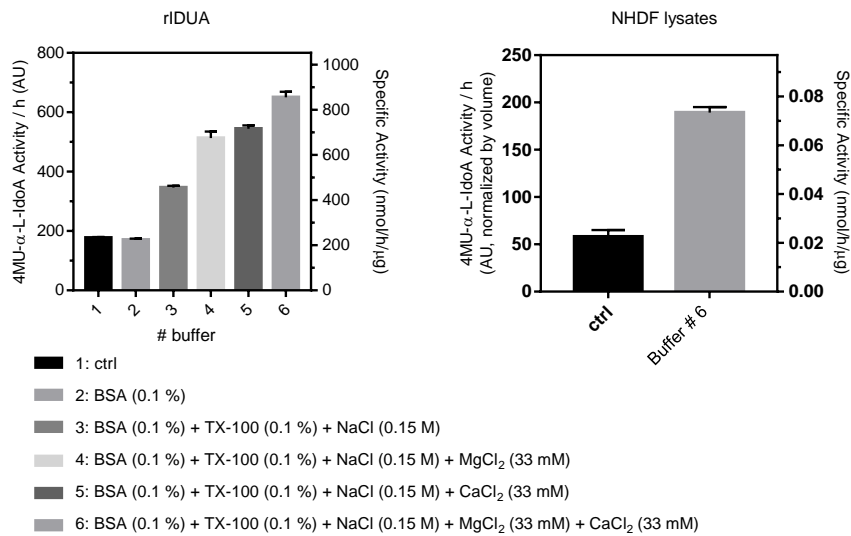


Figure 5.S1. Optimization of assay buffers for IDUA activity. Error range = SD from technical triplicates.

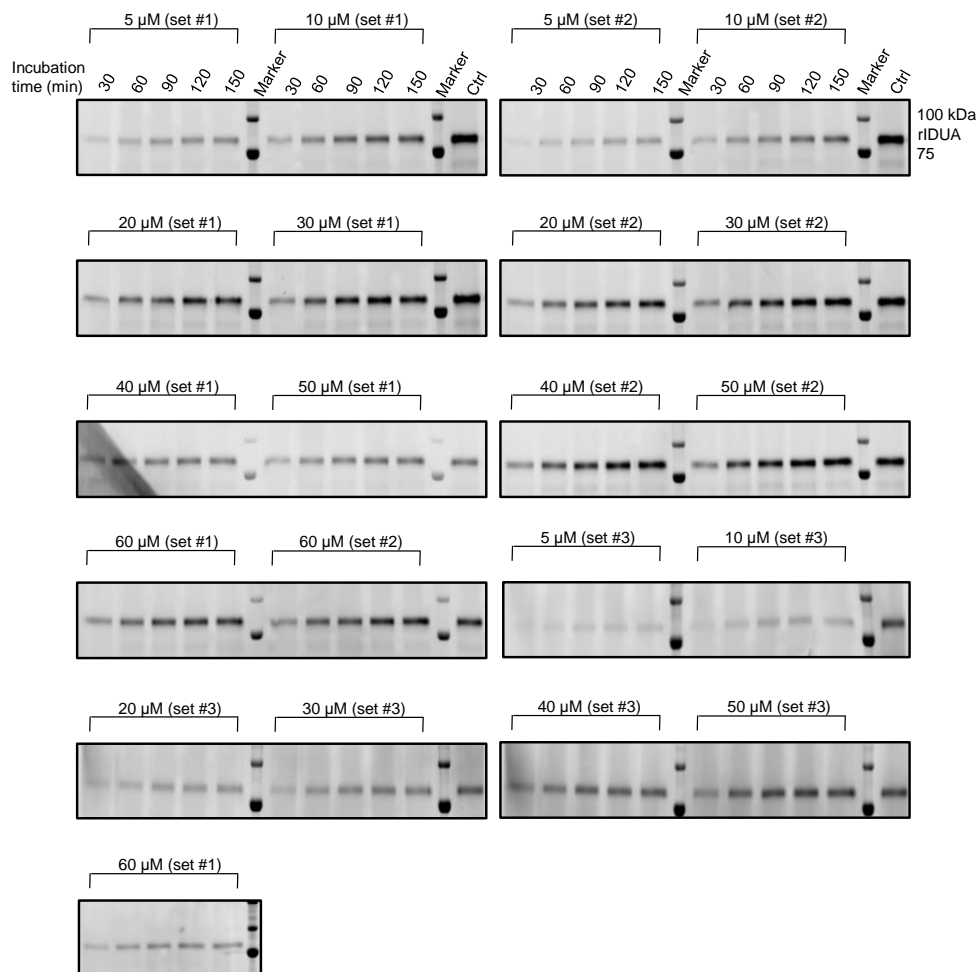


Figure 5.S2. SDS-PAGE gels used for labeling kinetic studies of ABP 2 with rIDUA. rIDUA was labeled at different incubation time periods (30–150 min) and at different ABP 2 concentrations (5–60 μM), before SDS-PAGE and fluorescent detection and quantification. The labeling experiment was performed in triplicate sets.

ABPs for α -L-iduronidase

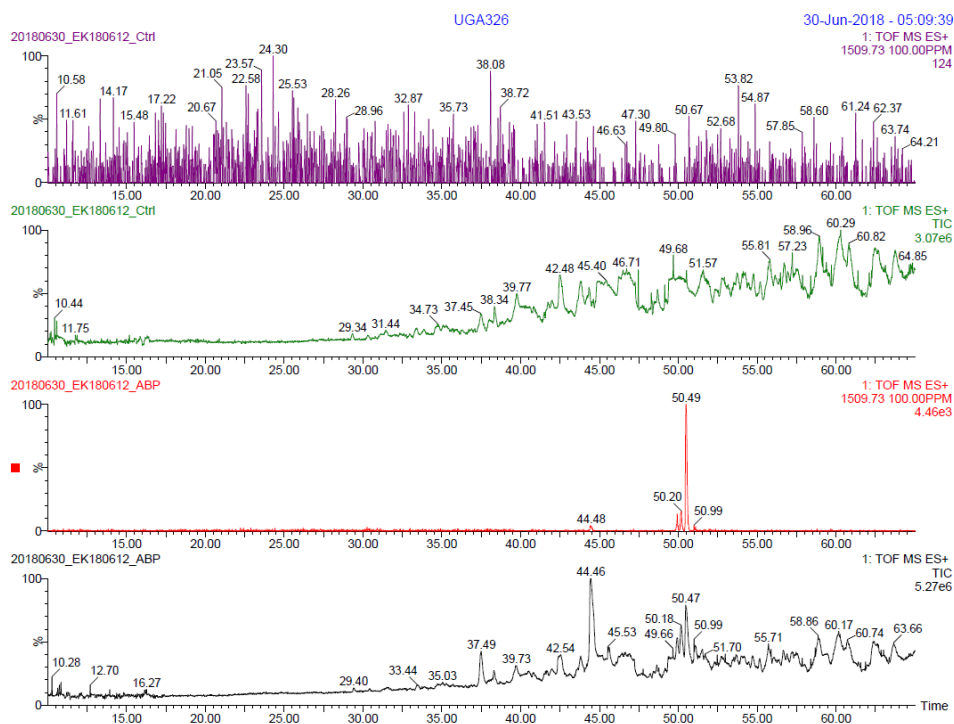
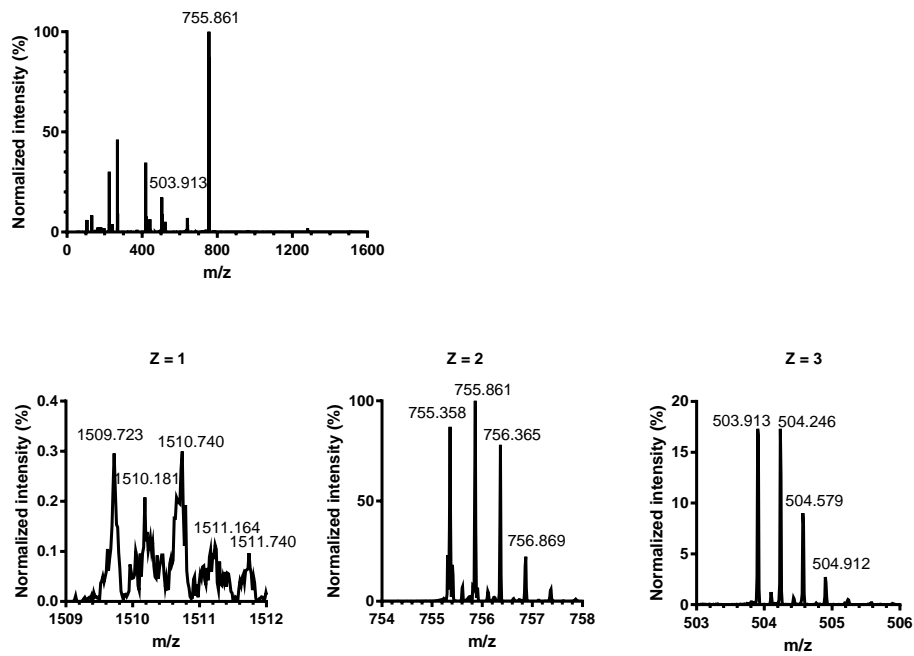


Figure 5.S3. Chromatogram of sample containing rIDUA active site peptide labeled without (Ctrl) or with ABP 3.

A



B

z	Theoretical		Experimental		Delta	ppm	
1	1509.725	1510.729	1509.723	1510.740	0.9999	1.52	7.28
2	755.3663	755.868	755.3578	755.8612	0.0534	11.25	9.00
3	503.9133	504.2478	503.9127	504.2455	0.3328	1.19	4.56

Figure 5.S4. LC-MS/MS identification of IDUA peptides labeled with ABP 3. A) Mass spectrum of sample containing rIDUA active site peptide labeled with ABP 3. B) Theoretical and experimental m/z values for rIDUA active site peptide labeled with ABP 3.

ABPs for α -L-iduronidase

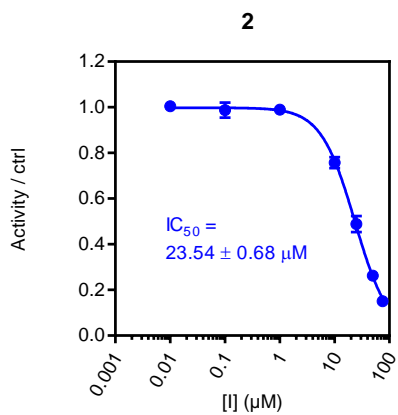


Figure 5.S5. Inhibition curve of ABP 2 on IDUA activity from NHDF lysates. Error range = SD from technical triplicates.

Table 5.S1. Data collection and refinement statistics for ralDUA in complex with fragments of 1 and 3.

	ralDUA in covalent complex with fragment of 1 (PDB: 6I6R)	ralDUA in non-covalent complex with fragment of 3 (PDB: 6I6X)
Data collection		
Space group	<i>P</i> 2 ₁ 2 ₁ 2 ₁	<i>H</i> 3
Cell dimensions		
<i>a</i> , <i>b</i> , <i>c</i> (Å)	206.9, 69.9, 93.7	259.2, 259.2, 71.0
α , β , γ (°)	90.0, 90.0, 90.0	90.0, 90.0, 120.0
Resolution (Å)	66.25-2.02 (2.05-2.02)	29.73-2.39 (2.44-2.39)*
<i>R</i> _{merge}	0.164 (1.047)	0.124 (0.866)
<i>R</i> _{pim}	0.080 (0.50)	0.061 (0.433)
<i>I</i> / σ	5.4 (1.3)	10.2 (1.3)
Completeness (%)	94.4 (97.8)	99.6 (94.0)
Redundancy	4.9 (5.0)	5.2 (4.8)
CC _{1/2}	0.99 (0.54)	0.995 (0.669)
Refinement		
Resolution (Å)	66.25-2.02	29.73-2.39
No. reflections	80558	66351
<i>R</i> _{work} / <i>R</i> _{free}	0.21 / 0.24	0.21 / 0.23
No. atoms		
Protein	9658	9818
Ligand	26	14
Water	250	294
<i>B</i> -factors		
Protein	38.6	43.2
Ligand	45.3	59.8
Water	35.2	39.2
Overall		
R.M.S. deviations		
Bond lengths (Å)	0.012	0.010
Bond angles (°)	1.56	1.45

*Values in parentheses are for highest-resolution shell.

5.S2 Synthesis of α -L-iduronic-configured inhibitors and ABPs (Department of Bio-organic Synthesis, Leiden University)

5.S2.1 General experimental details

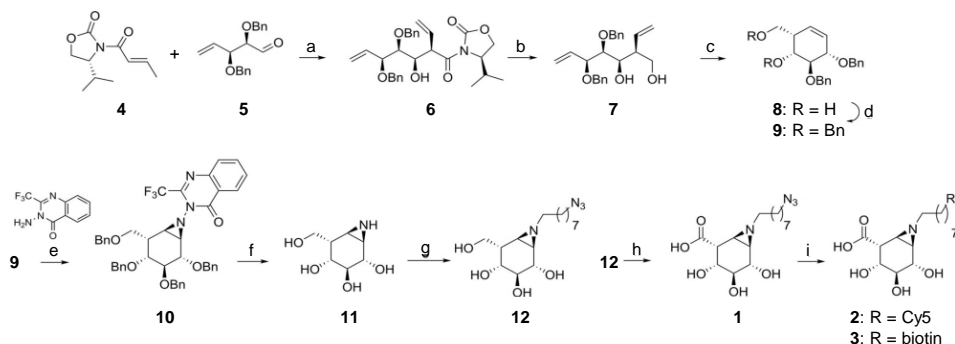
All reagents were of a commercial grade and were used as received unless stated otherwise. Dichloromethane (DCM), tetrahydrofuran (THF) and *N,N*-dimethylformamide (DMF) were stored over 4 Å molecular sieves, which were dried *in vacuo* before use. Triethylamine was dried

ABPs for α -L-iduronidase

over KOH and distilled before using. All reactions were performed under an argon atmosphere unless stated otherwise. Solvents used for flash column chromatography were of pro analysis quality. Reactions were monitored by analytical thin-layer chromatography (TLC) using Merck aluminum sheets pre-coated with silica gel 60 with detection by UV absorption (254 nm) and by spraying with a solution of $(\text{NH}_4)_6\text{Mo}_7\text{O}_{24}\cdot\text{H}_2\text{O}$ (25 g/L) and $(\text{NH}_4)_4\text{Ce}(\text{SO}_4)_4\cdot\text{H}_2\text{O}$ (10 g/L) in 10 % sulfuric acid followed by charring at $\sim 150^\circ\text{C}$ or by spraying with an aqueous solution of KMnO_4 (7 %) and K_2CO_3 (2 %) followed by charring at $\sim 150^\circ\text{C}$. Column chromatography was performed manually using either Baker or Screening Device silica gel 60 (0.04 - 0.063 mm) or a Biotage IsoleraTM flash purification system using silica gel cartridges (Screening devices SiliaSep HP, particle size 15-40 μm , 60A) in the indicated solvents. ^1H NMR and ^{13}C NMR spectra were recorded on Bruker DMX-600 (600/150 MHz) and Bruker AV-400 (400/100 MHz) spectrometer in the given solvent. Chemical shifts are given in ppm relative to the chloroform residual solvent peak or tetramethylsilane (TMS) as internal standard. Coupling constants are given in Hz. All given ^{13}C spectra are proton decoupled. The following abbreviations are used to describe peak patterns when appropriate: s (singlet), d (doublet), t (triplet), qt (quintet), m (multiplet), br (broad), ar (aromatic), app (apparent). 2D NMR experiments (HSQC, COSY and NOESY) were carried out to assign protons and carbons of the new structures and assignment follows the general numbering shown in cyclohexene **9**. High-resolution mass spectra (HRMS) of intermediates were recorded with a LTQ Orbitrap (Thermo Finnigan) and final compounds were recorded with an apex-QE instrument (Bruker). Optical rotations were measured on a Anton Paar MCP automatic polarimeter (Sodium D-line, $\lambda = 589\text{ nm}$). LC/MS analysis was performed on an LCQ Advantage Max (Thermo Finnigan) ion-trap spectrometer (ESI+) coupled to a Surveyor HPLC system (Thermo Finnigan) equipped with a C18 column (Gemini, 4.6 mm x 50 mm, 3 μm particle size, Phenomenex) equipped with buffers A: H_2O , B: acetonitrile (MeCN) and C: 1% aqueous TFA, or an Agilent Technologies 1260 Infinity LCMS with a 6120 Quadrupole MS system equipped with buffers A: H_2O , B: acetonitrile (MeCN) and C: 100 mM NH_4OAc . For reversed-phase HPLC-MS purifications an Agilent Technologies 1200 series prep LCMS with a 6130 Quadrupole MS system was used equipped with buffers A: 50 mM NH_4HCO_3 in H_2O and B: MeCN.

5.S2.2 Synthetic strategies

Synthetic strategies to assemble cyclophellitol derivatives often involve different configurations of functionalized cyclohexenes as starting materials. Based on the synthesis of D-galacto- and L-fuco-configured cyclohexenes described by Llebaria and coworkers¹ and the Overkleeft group,² it was reasoned that reaction of debenzylated aldehyde **5**³ with chiral Evans' oxazolidinone **4** should provide the L-ido-configured cyclohexene by syn-aldol addition (**Scheme 4.S1**). Indeed, asymmetric aldol condensation catalyzed by dibutylboryl triflate at low temperatures (-78°C to -20°C) proceeded stereo-selectively to provide the desired aldol product **6** in 60 % yield. During the reaction, the non-reactive terminal alkene derived from isomerization of acrylamide **4** was observed as a major side product. Reduction of oxazolidinone **6** with LiBH_4 followed by Grubbs II-catalyzed metathesis afforded the desired L-ido-configured cyclohexene **8** in excellent yield.



Scheme 5.S1. Synthesis of α -L-iduronic-configured inhibitors and ABPs 1–3. Reagents and conditions: a) DBBT, Et_3N , CH_2Cl_2 , -78°C to -20°C , 5 h, 60 %; b) LiBH_4 , THF, RT, 2 h, 99 %; c) Grubbs II catalyst, CH_2Cl_2 , 40°C , 18 h, 98 %; d) BnBr , TBAI, NaH, DMF, RT, 18 h, 79 %; e) $\text{PhI}(\text{OAc})_2$, CH_2Cl_2 , RT 48 h, 43 %; f) Li, NH_3 , THF, -60°C , 1 h, 93 %; g) 8-azido-1-iodooctane, K_2CO_3 , DMF, 55°C , 24 h, **12**: 22 %; h) TEMPO, NaBr, NaOCl, H_2O , 0°C , 3 h, 14 %; i) CuSO_4 , NaAsc, RT, 18–48 h, **2**: 22 %, **3**: 34 %.

Thereafter, olefin aziridination of L-ido-configured cyclohexene **8** was attempted, with the specific aim of obtaining the α -stereoisomer. Llebaria and co-workers have recently reported the first *N*-aminoaziridine covalent glycosidase inhibitors, which were prepared by stereoselective hydrogen-bonding-guided aziridination using 3-amino-2-ethylquinazolin-4(3*H*)-one (Et-Q-NH₂).² Because such hydrogen-bond-mediated aziridination of cyclohexene **8** would generate

the undesired β -diastereoisomer, the free alcohol groups in **8** were benzylated with benzyl bromide and sodium hydride to generate cyclohexene **9**. When the direct azidination of **9** was performed with in situ generated $\text{CF}_3\text{-Q-NHOAc}$ complex, the desired α -aziridine **10** was obtained in 43% yield together with 32% recovered starting material (**Scheme 4.S1**). This result implied that hydrogen bonding is not required for a productive aziridination, provided that the double bond is freely accessible. Removal of the $\text{CF}_3\text{-Q}$ and benzyl groups was achieved in one step by Birch reduction using lithium and liquid ammonia at -78°C . After quenching the reaction with H_2O , $\text{CF}_3\text{-Q}$ -derived impurities precipitated and were filtered off. Aziridine **11** was purged of lithium hydroxide by cation-exchange chromatography with Amberlite H^+ resin, and the fully deprotected cyclitol aziridine was obtained in 93 % yield (**Scheme 4.S1**). The α -L-configuration of aziridine **11** was established by ^1H NMR analysis (**Section 4.S2**), and the experimental coupling constants were compared with the corresponding calculated values obtained from DFT calculations (**Section 4.S3**). Aziridine **11** was then alkylated with 8-azido-1-iodooctane and K_2CO_3 or acylated with 8-azido-octanoic acid and EEDQ to afford intermediates **12** or **13**, respectively, which were purified by reversed-phase column chromatography. Oxidation of C-6 proved to be challenging due to instability of the aziridine under acidic or basic conditions. Aziridine **1** was obtained in 14 % yield by oxoammonium-catalyzed oxidation, maintaining the reaction and HPLC-MS purification at basic pH. Final click reaction with Cy5- and biotin-substituted alkynes afforded the desired ABPs **2** and **3**.

5.S2.3 Synthesis and characterization data of compounds 1–3

For detail the reader is referred to the supporting information published in Artola *et al.*⁴

5.S3. DFT Calculations (Department of Bio-organic Synthesis, Leiden University)**5.S3.1 Geometry optimization**

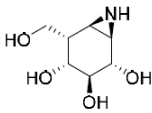
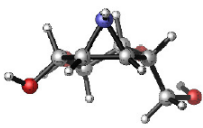
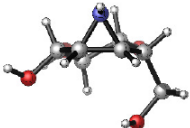
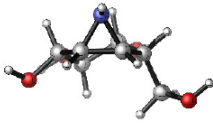
By using the conformer distribution search option included in the Spartan 14 program⁵, exclusively the 4H_3 conformation of the structure was found. Only notable variations of the geometry were found at the C5-C7 bond, including multiple rotamers which were significant higher in terms of energy. For α -L-idoA aziridine the 4H_3 conformation was also found as lowest energy conformer, but in this case the 3H_4 was only 1.4 kcal/mol higher in terms of energy.

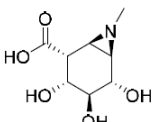
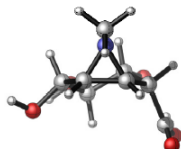
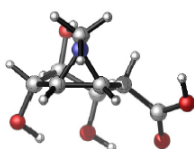
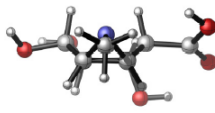
All calculations were performed with DFT as level of theory in combination with the B3LYP hybrid functional. A conformer distribution search option included in the Spartan 14 program⁵, in gas-phase with the use of 6-31G(d) as basis set, was used as starting point for the geometry optimization. All generated structures were further optimized with Gaussian 09⁶ at 6-311G(d, p). Optimization was done in gas-phase and subsequently corrections for solvent effects were done by the use of a polarizable continuum model using water as solvent parameter. The free Gibbs energy of the computed conformations was calculated using Equation (1) in which ΔE_{gas} is the gas-phase energy (electronic energy), ΔG_{RRHO}^T (T= 298.15 K and pressure= 1 atm.) is the sum of corrections from the electronic energy to free Gibbs energy in the rigid-rotor-harmonic-oscillator approximation (RRHO) also including zero-point-vibrational energy, and ΔG_{solv}^T is their corresponding free solvation Gibbs energy.

$$\begin{aligned}\Delta G_{aq}^T &= \Delta E_{gas} + \Delta G_{gas,RRHO}^T + \Delta G_{solv}^T \\ &= \Delta G_{gas}^T + \Delta G_{solv}^T\end{aligned}\tag{1}$$

The used free energies include unscaled zero-point vibrational energies. Visualization of the conformations of interest was done with CYLview.⁷

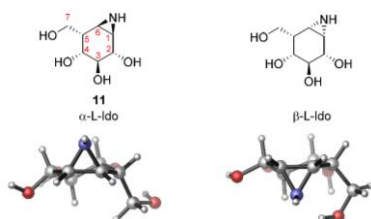
Table 5.S2. Geometry optimization of compound **11** and the *N*-methylated α -L-iduronic configured cyclophellititol aziridine performed by of DFT calculation.

 α -L- <i>ido</i> 11	 4H_3 <i>tg</i>	 4H_3 <i>gg</i>	 4H_3 <i>gt</i>
ΔG_{aq}^T (kcal/mol)	0.0	1.5	1.6
Geometry	D1: -45.4 °	D1: -43.4 °	D1: -45.6 °
	D3: -49.6 °	D3: -49.8 °	D3: -49.5 °
	D5: -2.3 °	D5: -3.1 °	D5: -3.0 °

 α -L- <i>idoA</i>	 4H_3	 3H_4	 $^{2,5}B$
ΔG_{aq}^T (kcal/mol)	0.0	1.4	8.0
Geometry	D1: -44.1 °	D1: 51.7 °	D1: -52.1 °
	D3: -53.5 °	D3: 43.8 °	D3: 48.0 °
	D5: -2.3 °	D5: 0.9 °	D5: 2.0 °

5.S3.2 NMR calculations

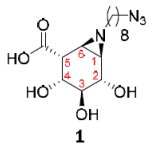
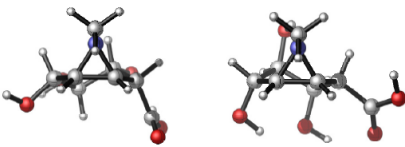
Based on the optimized lowest energy structure the spin-spin coupling constants were calculated according to the work of Rablen and Bally⁸ with the use of 6-311g(d, p) u+1s as basis set and PCM(H₂O) as solvent model and a scaling factor of 0.92. The calculated total nuclear spin-spin coupling terms were used as calculated spin-spin coupling constants.

Table 5.S3. Experimental coupling constants of α -idose configured cyclophellitol aziridine 12 compared to DFT calculated coupling constants.

H-H Coupling	Exp. $^3J_{(H,H)}$ (Hz)	α -L-ido DFT calc. $^3J_{(H,H)}$ (Hz)	β -L-ido DFT calc. $^3J_{(H,H)}$ (Hz)
H1-H6	6.0	5.8	6.8
H1-H2	n.d.	3.1	2.9
H2-H3	7.4	7.5	8.2
H3-H4	10.5	10.2	9.3
H4-H5	5.6	6.3	9.8
H5-H6	1.6	1.3	5.9
H5-H7a	4.4	2.8	0.9
H5-H7b	11.1	10.3	4.3

Coupling constants were determined by ^1H NMR experiments (exp.). n.d.: values not determine due to very small coupling constant ($J < 1$ Hz).

Table 5.S4. Experimental coupling constants of 1 compared to DFT calculated coupling constants of the methylated α -iduronic configured cyclophellitol aziridine.

				
H-H Coupling	Exp. $^3J_{(H,H)}$ (Hz)	α -L-idoA DFT calc. $^3J_{(H,H)}$ (Hz) 4H_3 (0.0 kcal/mol)	α -L-idoA DFT calc. $^3J_{(H,H)}$ (Hz) 3H_4 (1.4 kcal/mol)	α -L-idoA Boltzmann- weighted average $^3J_{(H,H)}$ (Hz)
H1-H6	n.d.	6.0	6.2	6.0
H1-H2	-	0.0	1.7	0.3
H2-H3	6.8	7.2	2.9	6.4
H3-H4	9.2-9.4	10.6	4.8	9.5
H4-H5	4.3-5.5	6.5	3.7	6.0
H5-H6	n.d.	1.7	0.8	1.5

Coupling constants were determined by ^1H NMR experiments (exp.). n.d.: values not determine due to peak overlap.

5.S4 Supplementary References

- 1 Hansen FG, Bundgaard E & Madsen R (2005) A short synthesis of (+)-cyclophellitol. *J Org Chem* **70**, 10139–10142.
- 2 Harrak Y, Barra CM, Delgado A, Castaño AR & Llebaria A (2011) Galacto-configured aminocyclitol phytoceramides are potent in vivo invariant natural killer T cell stimulators. *J Am Chem Soc* **133**, 12079–12084.
- 3 Jiang J, Kallemeijn WW, Wright DW, van den Nieuwendijk AMCH, Rohde VC, Folch EC, van den Elst H, Florea BI, Scheij S, Donker-Koopman WE, Verhoek M, Li N, Schürmann M, Mink D, Boot RG, Codée JDC, van der Marel GA, Davies GJ, Aerts JMFG & Overkleeft HS (2015) In vitro and in vivo comparative and competitive activity-based protein profiling of GH29 α -L-fucosidases. *Chem Sci* **6**, 2782–2789.
- 4 Artola M, Kuo CL, McMahon SA, Oehler V, Hansen T, van der Lienden M, He X, van den Elst H, Florea BI, Kermode AR, van der Marel GA, Gloster TM, Codée JDC, Overkleeft HS & Aerts JMFG (2018) New Irreversible α -L-Iduronidase Inhibitors and Activity-Based Probes. *Chemistry* **24**, 19081–19088.
- 5 Spartan '10 [Computer software]. (2010) Irvine, CA: Wavefunction Inc.
- 6 Gaussian 03 [Computer software]. (2004) Gaussian, Inc., Wallingford CT.
- 7 Legault CY (2009) CYLview 1.0b [Computer software]. Québec, Montreal, Canada: Univ Sherbrooke. Retrieved from <http://www.cylview.org>.
- 8 Bally T & Rablen PR (2011) Quantum-chemical simulation of ^1H NMR spectra. 2. Comparison of DFT-based procedures for computing proton-proton coupling constants in organic molecules. *Org. Chem* **76**, 4818–4830.

ABPs for α -L-iduronidase